直鎖アルキル基を持つ新規ポルフィリン

TTF化合物に関する研究

大阪教育

(1)

A Study on the Tetrathio-TTF Compounds Unsymmetrically Substituted with Normal Alkyl Groups

A Thesis

Submitted to

the University of Tokyo

in Fulfillment of the Requirement

for the Degree

of

Doctor of Science

(Rigaku Hakushi)

by

Akihiro Otsuka

December, 1990

to my parents

Acknowledgements

The present work has been carried out under the supervision of Professor Gunzi Saito. The author would like to express sincere gratitude to him for his continuous interest and valuable discussions and encouragement.

The author would like to express his thanks to Professor Minoru Kinoshita for his useful advice and valuable suggestions and discussions.

The author is grateful to Dr. Hideki Yamochi and Ms. Hatsumi Mori for their collaborations and helpful discussions and technical assistances. The author wishes to thank to Professor Tadashi Sugano, Mr. Kiyokazu Nozawa, Mr. Kenji Terui, Mr. Masafumi Tamura, and Dr. Philippe Turek for their helpful discussions and encouragement and technical assistances. The author would like to thank to Dr. Shoichi Sato for his helpful suggestions and discussions in the crystal structure investigations. The author greatly thanks to Professor Fumihiko Takei and all the members of his group for providing facilities for EPMA and X-ray measurements. The author wishes to thank to Mr. Kazuhiro Ohmichi, Dr. Seiichi Miyajima, and Professor Takehiko Chiba for their collaborations. The author wishes to thank to Ms. Toshiko Seki and Ms. Kimiyo Saeki for elemental analyses.

The author is heartily indebted to Dr. Norimichi Kojima and Mr. Toshiro Ban for their encouragement and helpful suggestions and discussions.

The author is gratefully indebted to Dr. Takayoshi

Nakamura, Dr. Mutsuyoshi Matsumoto, and Dr. Yasujiro Kawabata for their collaborations and valuable discussions, and for providing opportunity of LB films investigations in their laboratory.

The author gratefully acknowledges his debt to Dr. Kazumasa Honda, Dr. Midori Goto, and Dr. Masayasu Kurahashi for their sincere collaborations in the investigations of the crystal structures.

The author is very grateful to Professor Michiko Konno, Ms. Kazuyo Ohfuchi, Ms. Mariko Ito, and the other members of Professor Konno's group for their collaborations in the crystal structure investigations.

The author is heartily grateful to Professor Seiichi Kagoshima for his collaboration and helpful discussions in diffuse X-ray scattering studies at low temperatures.

The author greatly thanks to Professor Norio Isa for his collaboration and valuable discussions in mass spectra measurements.

The author wishes to express his thanks to Professor Atsushi Fujimori for his collaboration and helpful discussions in ESCA measurements.

The author is grateful to Dr. Takehiko Mori, Dr. Kenichi Imaeda, and Ms. Chikako Nakano for their useful advice and discussions.

Thanks are given to all the members of the laboratories of Professors Gunzi Saito and Minoru Kinoshita for their encouragement and various discussions.

Contents

1. Introduction

1-1. Control of the Physical Properties of a Molecular Assembly

How can we "control" the physical properties of a molecular assembly? In other words, what are the requirements to obtain a molecular assembly possessing a certain "intended" physical property? The general solution of this problem can be considered to be one of our goals, and it is of course worth while trying to make any step forward in that subject.

The approach to the synthesis of a material revealing the desired properties could formally consist of the following two steps. The first step is to "design" the molecular assembly. This is no other than to make clear what kind of molecular arrangements and electronic states are essential to the physical properties in question. The second one is to "construct" actually the designed assembly from its components. This step means an intended synthesis of a molecular assembly so as to control the molecular arrangements and electronic states.

In order to design and construct a molecular assembly in such a way, it should be required not only to understand correctly and precisely the intermolecular interactions working in the assembly, but also to control them freely. One of the practical methods is to introduce chemical

perturbations into a system and study their effects on its physical properties.

This thesis focuses on conductive organic molecular assemblies, and aims at the exploration of the new compounds in which the intermolecular interactions linking to the conducting properties could suffer chemical perturbations.

In choosing C_nTET-TTF (bis(alkylthio)ethylenedithio-tetrathiafulvalene, Fig. 1-1) as the object of study, BEDT-TTF (bis(ethylenedithio)tetrathiafulvalene) cation radical salts and TTC_n-TTF (tetrakis(alkylthio)tetrathiafulvalene) are briefly looked over in the next section.

1-2. BEDT-TTF Salts and TTC_n-TTF

BEDT-TTF (Fig. 1-1) was synthesized in 1978[1] in a course of the extension of TTF (tetrathiafulvalene) family.

It was not until $(BEDT\text{-}TTF)_2ClO_4(TCE)_{0.5}$ (TCE is 1,1,2-trichloroethane) was prepared in 1982[2] that this electron donor was highlighted. This cation radical salt maintained its metallic conduction and two dimensional conducting property down to 1.4 K[2]. It has been understood that its two-dimensional electronic property is based on its two-dimensional structural feature; the characteristic sulfur to sulfur atomic contacts along the side-by-side direction of the donor molecule[3].

In 1983, $(BEDT\text{-}TTF)_2ReO_4$, the first BEDT-TTF based organic superconductor (4 kbar, T_c=2 K) was reported[4]. Up to now, BEDT-TTF generated more than twenty superconductors. The highest T_c organic superconductor also belongs to the BEDT-TTF cation radical salts (0.3 kbar, 12.8 K for $(BEDT\text{-}TTF)_2Cu[N(CN)_2]Cl$[5]).

It is worth noticing that the following features are common to the conducting BEDT-TTF cation radical salts.

i) The donor molecules do not show a good planarity; the terminal ethylene groups, which belong to the six-membered ring, deviate from the C_6S_8 plane defined by the tetrathio-TTF part. The conformational disorders of the

ethylene groups are often observed. Such situations tend to prevent the direct face to face overlappings of the donor molecule. The intermolecular interaction in the side-by-side direction is as important as that along the normal of the molecular plane, or more.

ii) The concepts of "stacking column" are not necessarily suitable for describing the packing manner of the donor molecule. In most cases, the donor molecule is aligned with its long molecular axis almost parallel each other so as to produce a two dimensional conducting "sheet". This donor sheet is sandwiched in the insulating sheets consist of the counter anions, and the anion sheet is also between the donor sheets. The insulating sheet is made of discrete or polymeric ions and/or solvents. In some cases, the anions with novel structures are in situ incorporated into the salts.

iii) Analyzing the donor sheets in detail, various kinds of molecular arrangements are observed.[7] This polymorphism can give the samples of the same composition but different crystal structure, even in the same batch.

The features i) and ii) are considered to be strongly related with the two dimensional metallic state of those salts. The experimental evidences for closed Fermi surfaces (Schubnikov de Haas effect) have been observed in some BEDT-TTF salts.[8] The quasi-isotropic electronic character in

the conducting sheet must be making a great contribution to the stable metallic state and probably to the appearance of the superconductivity.

The wide variety of packing manners of BEDT-TTF salts mentioned in iii) leads to both possibilities and difficulties to control the physical properties. BEDT-TTF molecule is considered to have an ability to adapt to its circumstances, however, the molecules (which include anionic species) are automatically assembled by themselves. As a result, unless we clarified the mechanisms or conditions of the assembly formation, or unless we were able to directly touch the organizing processes of the components, it would be impossible to control the molecular arrangements and physical properties. At this stage, we are able to get some cation radical salts but unable to know their properties (e.g. semiconductor, metal or superconductor) before they are measured.

TTC_n-TTF is a series of tetrathio-TTF derivatives which has four normal alkyl substituents (n refers to the number of carbon atoms for one alklyl chain; Fig. 1-1).

TTC_1-TTF was first synthesized in 1974 through a potentiostatic reduction of 2-ethylthio-4,5-bis(methylthio)-1,3-dithiolium salt.[9] A lot of its charge transfer complexes and cation radical salts have been reported so

far, but a metallic behavior has been observed only on $(TTC_1\text{-}TTF)I_{2.47}$[10].

In $(TTC_1\text{-}TTF)I_{2.47}$, the donor molecule is almost flat including the terminal methyl groups. The donors pile up in parallel to make a conducting column. The side-by-side interdonor interactions are prevented by the methyl groups pointing to that direction as well as by anions. Instead, relatively short sulfur to sulfur distances are observed in the direction parallel to the long molecular axis. Such a donor packing in $(TTC_1\text{-}TTF)I_{2.47}$ is suggestive of a large difference between TTC_1-TTF and BEDT-TTF in the donor's ability to make a two dimensional conducting sheet.

The elongation of the normal alkyl chains, namely, the syntheses of the new molecules of TTC_n-TTF ($n=2\sim18$) were performed.[11] This chemical modification was regarded as the most basic and the simplest one aiming at some novel properties. The systematic investigations on TTC_n-TTF showed that its physical properties (conducting,[12] thermal,[13] and electronic[14]) and molecular and crystal structures[15] depend on the length of an alkyl chain.

n dependence of melting points shows the minimum (m.p.=24.6 °C for n=4). According to a thermodynamic analysis, TTC_n- TTF can be regarded as a flexible molecule as a whole like an alkane when $n\geq6$. This means that the cohesion is mainly dominated by the four alkyl chains in the

large n region (n≥6).

Electrical resistivity for TTC_n-TTF decreases ($10^{10}\rightarrow10^{5}$ Ωcm) with the increase in n (1→10). Connecting with the results of structure determination (vide infra), this phenomenon has been understood to be due to the increase in carrier mobility by an effective formation of conducting path.

For small n (n=1 (phase 1), 2, 3), the C_6S_8 segment is bent in a boat-form and the four alkyl chains are directed to the same side of the molecular plane. The molecules are packed in an unfavorable manner for electrical conduction. When n is more than three, TTC_n-TTF molecule now takes a chair-form with its C_6S_8 segment flat. The four alkyl chains are symmetrically directed in parallel to the opposite side of the C_6S_8 plane (Fig. 1-2). The whole alkyl chains in the crystal are aligned in parallel, and the rest (i.e. the C_6S_8 segments) is also made to be uniformly arranged to increase the intermolecular overlap integrals.

In this case, the C_6S_8 segments are directly responsible for the intermolecular interaction which affects the conducting property. On the other hand, the alkyl chains directly affect the arrangements of the C_6S_8 segments. This means that one can control the physical properties of TTC_n-TTF to some extent by changing n.

Although TTC_n-TTF is a single component conductor, it

can suffer a chemical perturbation from its alkyl chains and it presents a contrast to BEDT-TTF salts in which BEDT-TTF is not directly touchable.

1-3. Scope of This Thesis

The purpose of this work is to open up the novel group of conductive organic molecular assemblies of which physical properties could suffer chemical perturbations through the medium of intermolecular interactions.

C_nTET-TTF (Fig. 1-1) compound has been selected as the object of this study, because it is expected to have the characters of its both parent molecules (see section 1-2), and to show the ability to be controlled by its alkyl chains not only in a neutral state but also in a cation radical salt. As a matter of course, it is also very interesting to investigate its physical and chemical properties at the heterogeneous systems, for example Langmuir-Blodgett films. A part of such studies by us on C_7TET-TTF compounds were already presented.[15)]

This thesis consists of three chapters.

In chapter 2, the syntheses of C_nTET-TTF and the properties as a single component substance are described, making comparison with TTC_n-TTF series. The molecular and crystal structures of C_1TET-TTF are also presented in connection with its low resistivity (10^5 Ωcm).

In chapter 3, the preparation of cation radical salts of C_nTET-TTF is described in the first. The crystal

structures, conducting and EPR properties are shown on some of C_1TET-TTF salts which include a rare example of Sb_2F_{11} salt. The conducting properties on some C_2TET-TTF salts are also presented.

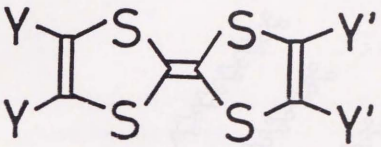

C_nTET-TTF	YY=-S(CH_2)$_2$S-, Y'=SC_nH_{2n+1}
TTC$_n$-TTF	Y=Y'=SC_nH_{2n+1}
BMDT-TTF	YY=Y'Y'=-S(CH_2)S-
BEDT-TTF	YY=Y'Y'=-S(CH_2)$_2$S-
BPDT-TTF	YY=Y'Y'=-S(CH_2)$_3$S-
trimethylene-TTF	YY=-(CH_2)$_3$-, Y'=H
MDT-TTF	YY=-S(CH_2)S-, Y'=H
EOET-TTF	YY=-O(CH_2)$_2$O-, Y'Y'=-S(CH_2)$_2$S-

Fig. 1-1. Structures of the compounds.

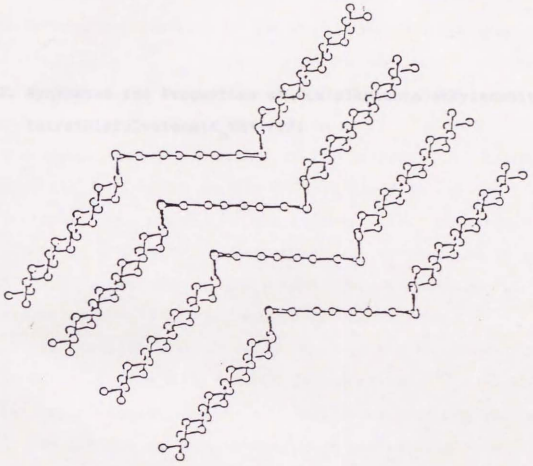

Fig. 1-2. Schematic representation of TTC_{10}-TTF; a side view of the stacking column.

2. Syntheses and Properties of Bis(alkylthio)ethylenedithio-tetrathiafulvalene(C_nTET-TTF)

2-1. Introduction

Some convenient reviews on the syntheses of TTF derivatives and their related compounds are available.[33)]

Tatemitsu et al. first synthesized C_1TET-TTF by the cross coupling reaction of the dithiolium tetrafluoroborates (Scheme 2-1a).[29)] They reported almost equal values of redox potentials for C_1TET-TTF, TTC_1-TTF, and BEDT-TTF with each other. Wu et al. also synthesized C_1TET-TTF through the cross coupling reaction of the ketones by trimethyl phosphite, and described its melting point as 122~126 °C.[34)]

After our reports on the syntheses and properties of C_7TET-TTF compounds[30)], Richard et al. synthesized C_{12}TET-TTF and C_{18}TET-TTF by the cross coupling reaction of the ketones according to the same procedure as ours.[31)]

Papavassiliou et al. also reported the three different synthetic routes to C_1TET-TTF (Scheme 2-1b).[19)] Although they are fundamentally based on the cross coupling reactions of the ketones and the thiones, the separations from their symmetrical products were improved with introductions of polar substituents into the intermediates. Two melting points for C_1TET-TTF were reported by them (Scheme 2-1b), independently of our result[15)] (79.2~80.2 °C, red).

As for TTC_1-TTF, crystallographically different two phases have been reported. The phase 1 is orange in color,

and the C_6S_8 segment of the molecule takes a boat-form in it.[21a] The physical properties of the phase 1 have been extensively studied as a member of TTC_n-TTF. Endres reported that the phase 2 of free TTC_1-TTF crystallized in red plates together with an unidentified product when an acetonitrile solution containing copper(II) acetate was evaporated on a slightly warm plate.[21b] The molecule is flat in the phase 2 except that two methyl groups are standing out from the plane. Any physical properties including melting point on the phase 2 has never been reported so far.

Wang et al. explained the alkyl chain length dependence of the melting temperature of TTC_n-TTF by analyzing the enthalpy and entropy changes at the melting point.[13b] They expressed the melting point T_m by the following equation

$$T_m = \frac{H_0 + nH}{S_0 + nS}$$

$$= \frac{H}{S}\left(\frac{H_0/H - S_0/S}{n + S_0/S}\right)$$

where n was the number of the carbon atoms within a alkyl chain, and H_0+nH and S_0+nS were the enthalpy and entropy changes at the melting point, ΔH_m and ΔS_m, respectively.

According to this hyperbolic function of n, T_m shows a decreasing curve with n in the case of $(H_0/H)>(S_0/S)$, while in the case of $(H_0/H)<(S_0/S)$, T_m shows an increasing curve with n. The appearance of a minimum in the melting point of TTC_n-TTF has been ascribed to the change of the difference in magnitudes between (H_0/H) and (S_0/S) as a function of n. They have interpreted it as a result of the concurrence of two kinds of interactions, which arise from the π-like electronic part and the alkyl part.

Mori et al. have calculated on the electronic states of the alkyl-substituted C_6S_8 molecules.[10), 14a), 32)] The ratio of the atomic populations of the HOMO between the outer sulfur atoms and the inner ones (P_{out}/P_{in}) were given; 0.05 for TTC_1-TTF (phase 1) and TTC_n-TTF (n=2 and 9), 0.1 for BPDT-TTF, 0.148 for BEDT-TTF, 0.315 for BMDT-TTF, and 0.452 for TTC_1-TTF in $(TTC_1\text{-TTF})I_{2.47}$. It seems that the relative importance of the outer sulfurs is increased as the π-like electrons on the C_6S_8 segment become able to spread out.

In this chapter, the syntheses, some physical, chemical, and structural properties of C_nTET-TTF (n=1, 2, 4, 7, 10, 13, 16, and 18) are described and compared with those of TTC_n-TTF and BEDT-TTF. The cation radical salts of these compounds will be treated in Chapter 3.

2-2. Syntheses of C_nTET-TTF

Synthetic scheme of C_nTET-TTF is shown in Scheme 2-2. It is composed of a random coupling reaction between the ketones by triethyl phosphite ($P(OEt)_3$).

The experimental procedure for C_7TET-TTF is shown below as a representative. A mixture of 1.11 g (5.34 mmol) of 4,5-ethylenedithic-1,3-dithiole-2-one and 2.20 g (5.34 mmol) of 4,5-bis(heptylthio)-1,3-dithiole-2-one was warmed in 3.74 g (22.5 mmol) of freshly distilled $P(OEt)_3$ under argon at about 100 °C for 24 h. Addition of methanol to the cooled reaction mixture precipitated oily brown product, which was collected on a fine glass filter (G4) and washed with methanol then gave 2.20 g of oily dark brown powder. Washing the oily powder with n-hexane left BEDT-TTF as an orange powder(0.50 g) on the filter. The n-hexane filtrate was concentrated and chromatographed (silica gel, n-hexane) to give yellowish orange crystals of TTC_7-TTF (0.67 g) and a reddish orange oil of C_7TET-TTF (0.68 g).

C_7TET-TTF:mp=11.4~13.4 °C (reddish orange oil, yellow crystals). Anal. Found:C, 47.82; H, 6.36; N, 0; S, 46.32%. Cald for $C_{22}H_{34}S_8$:C, 47.61; H,6.17; S, 46.21%. EI-MS m/e:554(M^+), 236(M^+-$C_{16}H_{30}S_3$), 208(236-C_2H_4); the isotope pattern of the parent peak agreed with the calculated one. λ_{max}(lg(ε/dm^{3}mol^{-1}cm^{-1}) in $CHCl_3$):302(sh, 4.09), 316(4.13),

343(4.10), 385(sh, 3.48), 480 nm(sh, 2.46). IR(neat):2960(m), 2930(s), 2850(m), 1465(w), 1455(w), 1412(w), 1375(w), 1284(w), 918(w), 885(w), 772(m), 723(m) cm^{-1}. ^{1}H-NMR($CDCl_3$, TMS, 60 MHz):δ=3.28(s, 4H), 2.80(t, 4H), 1.51(m, 20H), 0.88(t, 6H) ppm. The purity was checked by TLC and HPLC (silica gel).

The solvents used for the purification were altered depending on the solubility of the products. For n=4 and 7, C_nTET-TTF is reddish orange oil at room temperature and purified only by silica gel column chromatography (n-hexane). Florisil and neutral alumina were tried for adsorbent of column chromatography on C_7TET-TTF, but both were found to bring some decomposition. As eluent for chromatography, n-hexane-diethyl ether was used for n=1 and 2, and n-hexane-benzene for n=10, 13, 16 and 18. Further recrystallization was performed from methanol for n=1, n-hexane-benzene for n=2, and n-hexane for n=10, 13, 16, 18. The addition of charcoal had an evil effect on the recrystallization. Since the solubility of C_nTET-TTF decreases in the large n region (especially n=16 and 18), the polarity of the solvent for column chromatography has been selected with a great care so as not to precipitate C_nTET-TTF in the chromato column, and so as to give a sufficient separation as well. The further purification of C_1TET-TTF was tried by means of HPLC (GPC, chloroform), but

did not succeed.

The yields and melting points (mp) of C_nTET-TTF are summarized in Table 2-1. The yields (not optimized) were calculated assuming the complete random coupling reactions between the ketones mixed in 1:1 ratio. They were independent of the length of alkyl chains. BEDT-TTF was obtained almost quantitatively in the all cases examined.

The mp of C_4TET-TTF has not been determined yet. It should be lower than that of C_7TET-TTF (12°C) because C_4TET-TTF does not crystallize in the same condition in which C_7TET-TTF crystallizes (kept at -20 °C for two weeks). The color of C_nTET-TTF in solid state is from reddish orange to orange yellow. The n dependence of mp will be described in the next section (2-3).

To obtain the ketones, we have taken the different synthetic routes depending on the alkyl substituents (see Scheme 2-3).

For the normal alkyl groups (n=4, 7, 10, 13, 16, 18), the route (a) was successful which includes the half-opening process of 1,3,4,6-tetrathiapentalene-2,5-dione (TPD) by Na_2CO_3 with an alkyl ammonium phase transfer catalyst (Aliquat 336). This method is a direct application of Schumaker et al.'s procedure[16] to normal alkyl bromides. We obtained the ketones as brown liquid for n=4, 7 and as

pale brown solid for n=10, 13, 16, 18, in good yields (67, 81, 83, 62, 73, 63% based on TPD, respectively).

The experimental procedure for n=7 is shown below as a representative. The reaction was carried out under inert atmosphere. 10.2 g (49 mmol) of TPD was placed in a three-necked flask with a condenser, a thermometer and a dropping funnel. To this flask, 17.98 g (100 mmol) of heptyl bromide, 38.53 g (95 mmol) of Aliquat 336 and 600 cm^3 of benzene were added, and the mixture was degassed for 10 minutes by bubbling argon vigorously through the stirred mixture. An aqueous solution of anhydrous sodium carbonate (21.4 g (202 mmol) in 200 cm^3 of water) was added dropwise to the mixture with vigorous stirring under argon for 2 h at 44∿46 °C. This reaction was slightly exothermic, therefore the addition rate of sodium carbonate was controlled so as not to raise the temperature over 46 °C. The color of the reaction mixture changed from pale yellow to yellowish brown. After the reaction mixture was cooled, the organic layer was separated, washed with water (200 cm^3×3), dried over anhydrous Na_2SO_4 and the solvent evaporated, leaving a dark brown oil (50.82 g). The crude oil was chromatographed two times (silica gel, n-hexane), yielding a deep brown liquid:15.02 g (81% based on TPD); IR(neat)2960(m), 2935(m), 2865(m), 1755(w), 1670(s), 1610(w), 1465(m), 1458(m), 1375(w), 1300(w), 1270(w), 1245(w), 1225(w), 1200(w),

881(m), 722(w) cm^{-1}; MS, m/e 378.

For n=10, 13, 16, 18; mp(recryst.), 36.5∿37.6(column), 54.7∿55.3(benzene), 66.7∿67.2(acetone), 72.7∿73.2 °C(benzene -acetone), respectively.

The route (a) is more favorable than the route (b), because the former needs no mercury reagent. Unfortunately, this method was unsuccessful when 1,2-dibromoethane or methyl iodide was used as an electrophile in the same conditions. In the case of dibromoethane (ca. 20% yield based on TPD), the conversion of TPD into the product was incomplete (checked by TLC, IR and mass spectra), and the separation of the product from TPD was difficult due to a similar solubility. In the case of methyl iodide, there was one more difficulty on the reaction temperature (40∿46 °C) which is almost equal to the bp of methyl iodide (42 °C).

As for the small alkyl derivatives (R=Me or Et, RR=-CH_2CH_2-), we have taken the route (b) which starts from a zinc complex synthesized by a known method[17] from carbon disulfide. The thiones were directly obtained from the zinc complex in 70∿95% yields, and they were converted to the ketones by $Hg(OAc)_2$ in ca. 90% yields.

The experimental procedure for n=2 is shown below as a representative. 5.00 g (5.30 mmol) of $TBA_2[Zn(dmit)_2]$ and 28 cm^3 of acetone (dried over anhydrous $CaSO_4$) was mixed in a suspension under argon. To this red suspension, 3.6 g

(23.1 mmol) of ethyl iodide was added all at once (slightly exothermic), and stirred for 12 h in the dark at room temperature. The resulting deep green solution was evaporated to dryness, column chromatographed (silica gel, n-hexane:CH_2Cl_2=1:1), yielding a brown yellow oil:2.56 g (94.8% based on the zinc complex); IR(neat)2973(m), 2923(m), 2865(w), 1448(m), 1421(w), 1375(w), 1259(m), 1067(s), 1035(m), 967(w), 888(w), 762(w), 736(w), 515(m) cm^{-1}; MS, m/e 254.

A mixture of 6.42 g (25.22 mmol) of 4,5-bis(ethylthio)-1,3-dithiole-2-thione, 8.07 g (25.32 mmol) of $Hg(OAc)_2$, 80 cm^3 of chloroform, and 80 cm^3 of acetic acid was refluxed for 5 h. The color of the reaction mixture changed from yellow to yellowish green, dull green, dark green, then to black. After the mixture was cooled, black powder of HgS was filtered off (Na_2SO_4 over celite) by suction. The yellow filtrate was neutralized (Na_2CO_3 aq.), washed with water, dried over anhydrous $MgSO_4$, and the solvent evaporated, leaving a brown yellow oil:5.85 g (97.3% based on the thione); IR(neat)3324(w), 3270(w), 2976(s), 2925(s), 2868(m), 2825(w), 1825(w), 1760(s), 1668(s), 1613(s), 1478(s), 1448(s), 1423(s), 1376(s), 1259(s), 1122(m), 1056(m), 1039(m), 996(m), 966(s), 885(s), 765(m), 739(m), 671(w), 644(w), 552(m) cm^{-1}; MS, m/e 238.

For n=1 and RR=-CH_2CH_2-, the ketone was recrystallized

from diethyl ether and ethanol, respectively; mp, 57.2~57.7 and 127~128.5 °C, respectively.

2-3. Melting Points of C_nTET-TTF

The melting points of C_nTET-TTF are shown in Fig. 2-1 together with those of TTC_n-TTF and 4,5-bis(alkylthio)-1,3-dithiole-2-one.

In the case of TTC_n-TTF[13], it has been understood that the region of n is divided into the three (1, 2 and 3). In the region 1 ($1 \leq n \leq 4$), the central C_6S_8 segment govern the molecular packing, and the alkyl groups work only to disturb the attracting force among the molecules as n increases. In the region 3 ($n \geq 6$), the molecular packing is mainly dominated by the alkyl chains as if TTC_n-TTF is a flexible molecule like a n-alkane (C_nH_{2n+2}), and the intermolecular cohesion increases with increase in n. The region 2 is the intermediate one, and a minimum of the melting points is observed in this region (section 2-1).

It is noteworthy that such "V-shape" correlation between the melting points and the lengths of n-alkyl chain within a molecule is also observed on unsymmetrical molecules. Figure 2-2 shows the n dependence of the melting points and boiling points for normal alkyl substituted benzenes ($Ph\text{-}C_nH_{2n+1}$).[68] The boiling points increase monotonically with increasing n. This suggests that in the boiling process, the increase of n merely means the increase of the molecular weight. On the other hand, a minimum

appears in the n dependence of the melting points in common with TTC_n-TTF. Similar behavior of the melting points with n is known for 1- or 2-n-alkyl naphthalenes[18]. Figure 2-3 shows the melting and boiling points of n-alkanes (C_nH_{2n+2})[68), 69)] for comparison.

The melting points of C_nTET-TTF look to obey the similar n dependence to TTC_n-TTF. The melting point decreases with increasing n in the small n region, then, it shows a minimum (at $3 \leq n \leq 6$), and at n 7 it quickly increases as n increases. The similar behavior is observed on one of its coupling moieties, 4,5-bis(alkylthio)-1,3-dithiole-2-one.

C_nTET-TTF tends to show lower melting points compared with TTC_n-TTF at the same n. This is ascribable to both a decrease in the number of alkyl chains for a molecule and a reduction in the symmetry of a molecule (the enthalpy change at mp for C_7TET-TTF is about 7.3% of that for TTC_7-TTF, and entropy change is 8.1%, for example). In spite of such a drastic difference in the molecular structure, both compounds look to give their minima of melting points in almost the equal n region. This suggests a great significance of a role of the non-alkyl part of the molecule in the solid state.

The appearance of the minimum in the n dependence of the melting points could have a general meaning that another

characteristic interaction works in the solid besides the interactions by n-alkyl groups. In the above mentioned systems, the another interaction should be based on the π-electronic segments.

For C_1TET-TTF, there might be more than three phases in view of the melting points. Wu and Zheng described its melting point as 122∿126 °C (purified by silica gel chromatography and recrystallized in hexane).[34] Papavassiliou and co-workers have reported the melting points (64, orange and 75∿76 °C, red)[19] which are different from the value of Wu et al.s' and ours (80.2∿81.2 °C, red). They obtained the value of 64 °C when C_1TET-TTF was recrystallized from n-hexane including a slight amount of chloroform[20]. We have recrystallized from n-hexane:diethyl ether=4:1, acetonitrile, or methanol, and the melting points have converged to ca. 80 °C regardless of the color of the crystals. When the product was crude or it was recrystallized from cyclohexane, we detected the mp of 70∿76 °C. Two phases are reported for TTC_1-TTF by structure analyses[21], and $TSeC_1$-TTF by mp[22], resistivity[23] measurements and structure analyses[24].

Anyway, the melting points of C_nTET-TTF change depending on n. The molecular arrangement is expected to be controlled in the solid state as a function of the relative importance between alkyl groups and the rest.

2-4. Electrical Resistivities of C_nTET-TTF

The resistivities were measured by a two-probe or a quasi-four-probe dc-method using 10 or 20 μm-diameter gold wires with silver paste (Du Pont 4922) or gold past (Tokuriki 8560) as electrical contacts.

The samples were mounted in a glass cell (Fig. 2-4). To check the influence of oxygen, some measurements were performed on C_1TET-TTF and BEDT-TTF single crystals under a reduced pressure generated by an oil diffusion pump with liquid nitrogen traps. Almost no change of resistivity was observed even after the vacuum was maintained for more than 12 h. Therefore, the most measurements were done under ambient pressure of nitrogen gas after exchanging the atmosphere in the cell several times. The temperature was controlled between -15 and 60 °C by immersing the cell covered with aluminum foil into a water-ethylene glycol bath, and it was measured by a copper-constantan thermocouple placed just near the sample into the cell. The ohmicity was always confirmed, and the ranges of sensors (ammeter or voltmeter) were selected so as not to affect the measurements.

Figure 2-5 and Table 2-1 show the dc-electrical resistivities of C_nTET-TTF together with that of BEDT-TTF at room temperature. The data on TTC_n-TTF[12] are also plotted

on the same figure for comparison.

For $n \geq 2$, the resistivities of C_nTET-TTF decrease as n increases, then look to converge into a value of $10^6 \sim 10^7$ Ωcm with compaction pellets. Especially in the case of C_{10}TET-TTF, its value of 1.0×10^6 Ωcm in compaction is comparable to that of single crystal of TTC_{10}-TTF (3.7×10^5 Ωcm[12]). Such an n dependence of resistivity, in which the resistivity decreases as n increases, has been already observed on TYC_n-TXF series (Y=sulfur, selenium or tellurium for X=sulfur; Y=sulfur or selenium for X=selenium) and has been understood as "molecular fastener effect" (section 1-2).

C_nTET-TTF has only two normal alkyl chains, and the π-electronic segment is placed at the other end of the molecule. This forms a striking contrast to TTC_n-TTF in which the C_6S_8 segment is placed at the center of the molecule. It is not difficult to imagine that the four alkyl chains fasten up the central C_6S_8 π-electronic system so as to make a conduction path in the crystal of TTC_n-TTF. In the case of C_nTET-TTF, such a concept of "fastening" by alkyl chains might be unsuitable for the explanation of its low resistivity considering its molecular skeleton. Of course the structure analyses on single crystals of C_nTET-TTF (for $n \geq 10$) are necessary to understand what happening.

Since the single crystals of C_{10}TET-TTF have not been obtained, we have conjectured its rough molecular packing by

means of powder X-ray diffraction. Figure 2-6 shows a part of the diffraction pattern for C_{10}TET-TTF. There exists a series of diffraction peaks (n=1~6) which corresponds to a repeating unit of 38 Å. Considering that TTC_{10}-TTF[58] has a distance of d_{010}=32.77 Å between the ac planes, it is likely that C_{10}TET-TTF also crystallizes to form a sheetlike structure in which the molecules are arranged in a head to head manner (see Fig. 2-7).

If it was the case that C_nTET-TTF ($n \geq 10$) is packed such as Fig. 2-7 (b), its low resistivity should be ascribed to the substantial packing arrangement of the C_6S_8 segment with ethylene group in the crystal and not to so-called "a fastener effect". Since the flatness of the C_6S_8 segment is considered to be poor on the analogy of C_1TET-TTF (section 2-5) and C_7TET-TTF (Fig. 2-8), the interactions in the side-by-side direction of the molecule must play an important role in the electrical conduction compared with TTC_n-TTF.

Single crystals, which have been obtained for n=1, 2 and BEDT-TTF, show the resistivities smaller by a factor of almost two than those of their compaction specimens respectively. The remarkable fact is that C_1TET-TTF single crystals show the smallest resistivity among these compounds. The value of $\rho_{rt}=5.4\times10^5$ Ωcm is nearly equal to that of TTC_{10}-TTF (3.7×10^5 Ωcm[12]) which is the smallest one among the single component organic semiconductors made from

carbon, sulfur, and hydrogen only. This implies that C_6S_8 segment with ethylene group has a potential ability to produce a conductor by itself, without the assists by long alkyl chains. BEDT-TTF single crystals also show the relatively small value of 2.6×10^7 Ωcm.

In the case of TYC_n-TTF (Y=tellurium[12), 25)] or selenium[23)], the molecule of n=1 tends to give the crystal of high electrical conductivity as much as that of its large n derivatives. It was revealed that characteristic tellurium atomic contacts play an important role in $TTeC_1$-TTF single crystals.[25)]

C_1TET-TTF dose not contain the larger chalcogen atoms than sulfur, therefore the character of the molecule is expected to come to the fore even in its assembly. The molecular and crystal structures of C_1TET-TTF are described in the next section in comparison with those of BEDT-TTF and TTC_n-TTF.

2-5. Molecular and Crystal Structures of a Low Resistivity Single Component Organic Conductor; C_1TET-TTF

X-Ray crystal structure analysis was carried out for C_1TET-TTF single crystals. The diffraction data were collected at room temperature by use of an automated four-circle diffractometer, Rigaku AFC-5 with a graphite monochromated Mo radiation (Mo Kα =0.71069 Å). Crystallographic data are listed in Table 2-2. Crystal structure was solved by a direct method using MULTAN program system and was refined by the full-matrix least-squares program. Anisotropic temperature factors were used for the refinement of the non-hydrogen atoms. The final atomic parameters are listed in Table 2-3.

Molecular Structures

Crystallographically independent two molecules (I and II) are observed in the crystal. The molecular structures and bond lengths of them are shown in Fig. 2-9 together with the numbering of atoms. The C_6S_8 segment of the both molecules takes a boat-form (bending angles are 13.3 and 10.0° for I, 17.5 and 5.5° for II, respectively, Fig. 2-10).

We can point out delicate differences between I and II on their outer alkylthio groups. For useful information, the molecular side views of TTC_1-TTF (phase 1)[21a], TTC_1-TTF

(phase 2)[21b], and BEDT-TTF[26] are shown in Fig. 2-11.

One of the two methyl groups of II (Fig. 2-10) stands almost normal to the molecular plane, but another methyl carbon lies in that plane. On the other hand, both methyl carbons of I are placed in the intermediate positions between them. It is interesting to notice that the conformations of methylthio groups of I resemble those of TTC_1-TTF (phase 1), and those of II resemble those of TTC_1-TTF (phase 2), respectively.

Such structural correlations to the parent molecule are also recognized on ethylenedithio groups. The both conformations in I and II (Fig. 2-10) exist in one molecule of BEDT-TTF.

Consequently, we observe all of the conformations of the alkylthio groups, which are known in TTC_1-TTF (phase 1 and 2) and BEDT-TTF, in one crystal of C_1TET-TTF. This may be quite natural, considering that C_1TET-TTF is a hybrid molecule between TTC_1-TTF and BEDT-TTF. However, if the present crystal is a mixed crystal of the molecule I and II, not only the respective pure crystals of I and II but also some novel structures may be obtained depending on the experimental conditions.

The bending of the C_6S_8 segment such as Fig. 2-10 might be a disadvantageous to getting a electrical conductor, because the extension of the π-orbitals' conjugation might

be reduced, and because the molecular arrangement might result in a looser packing.

As for the electronic states of a molecule, it is worth noticing the extended-Hückel molecular-orbital calculations on TTC_n-TTF (n=1, 2, and 9) with the geometry in its real crystal[14a]. They indicate that the molecular-orbital energies hardly depend on whether the C_6S_8 segment is bent or flat. This result might agree with the fact that the redox potentials of TTC_n-TTF in solution are independent of n[11]. Accordingly, the large differences in the solid state properties between TTC_1-TTF and TTC_{10}-TTF should be ascribed to the differences in the intermolecular interactions which are functions of their molecular packings (though the molecular packing is strongly influenced by the molecular structure of course).

If the above story remains valid for C_1TET-TTF which has the bent but the same C_6S_8 skeleton as the conjugation system, C_1TET-TTF molecule also should have an ability to form an electrical conductor as far as the grade of TTC_{10}-TTF. C_1TET-TTF in fact shows the low resistivity almost equal to that of TTC_{10}-TTF (section 2-4). The molecular packing suitable for the electrical conduction must be observed in this C_1TET-TTF crystal.

Crystal Structure

The crystal is monoclinic with space group $P2_1/c$. Figure 2-12 shows the crystal structure projected along the a axis. Eight molecules are contained in the asymmetric unit, and they are piled up along the b axis which is the longest crystallographic one (31.303(6) Å). The resistivity measurements were performed in the direction parallel to the most elongating axis of the crystals which was identified as the crystallographic a axis from X-ray oscillation photographs.

Relatively close intermolecular sulfur to sulfur distances, which are shorter than the upper limit of the sum of the van der Waals radii (3.7 Å), are found only among the molecules I. The molecule II, which is isolated in the crystal judging from atomic contacts, could not directly contribute to the electrical conduction, but it is actually one of the essential components of this conducting crystal.

The molecules are arranged side-by-side regularly along the a axis. Four short S··S distances (3.49~3.62 Å) for a molecule I are observed in that direction, and they are kept among one outer sulfur atom and two inner ones (Fig. 2-13). In the direction along the c axis, two close S··S distances (3.60 Å) for a molecule I are observed which are maintained among two inner sulfur atoms (Fig. 2-14).

As a result, the molecules I form the two-dimensional

sulfur to sulfur networks parallel to the ac plane. The molecules II are sandwiched between those sheets made of molecules I.

It is important to notice that the inner sulfur atoms, which are included in TTF skeleton and are expected to have the largest atomic population of HOMO (section 2-1), greatly participate in the formation of the S··S networks, as shown in Fig. 2-15. In the six contacts for a molecule, the four arise from the inner sulfurs.

Table 2-4. summarizes the manners of S··S networks and the conducting properties of C_1TET-TTF, TTC_1-TTF (phase 1 and 2), BEDT-TTF, and TTC_{10}-TTF for comparison.

What is common to C_1TET-TTF and TTC_{10}-TTF (both show the same order of resistivity, 10^5 Ωcm) seems to be the strong interactions among the conjugation systems. The close S··S networks through inner sulfur atoms look to play an important role in C_1TET-TTF. The close face to face stacking (3.49 Å) of the C_6S_8 plane with short S··S contact (3.57 Å) of inner sulfur atoms looks to contribute to the conduction in TTC_{10}-TTF.

BEDT-TTF molecules are dimerized in a face to face fashion with 3.69 Å distance between inner sulfur atoms. The dimers are arranged side-by-side regularly to form the dimers of chains along the a axis. In the eight S··S contacts (3.48∿3.69 Å) for a molecule, only three include

the inner sulfur atoms. Such differences in the quality of S··S networks from C_1TET-TTF would be responsible for the larger resistivity and activation energy. Nevertheless, the side-by-side regular arrangement of BEDT-TTF shows the resistivity smaller by a factor of three than that of TTC_1-TTF (phase 1).

TTC_1-TTF (phase 1) has a lot of S··S contacts (3.48∿3.66 Å)[27] only among the outer sulfurs on which sufficient atomic population could not be expected (section 2-1). What is worse, the molecular planes of the nearest neighbors are almost perpendicular to each other. This situation is quite disadvantageous to the close interactions among the conjugation systems.

The phase 2 of TTC_1-TTF also has S··S contacts (3.59 Å) only among the outer sulfurs. In contrast to the phase 1, the molecule is flat except for two methyl groups standing nearly perpendicular to the molecular plane. The molecules are stacked regularly, and the overlap pattern of two molecules within a stack is very reminiscent of that of TTC_{10}-TTF. However, the intermolecular separation seems to be larger, judging from that the shortest S··S distance (3.72 Å) between the planes is longer than that for TTC_{10}-TTF (3.57 Å).

From the above comparison with the related molecules, the characteristic feature of the C_1TET-TTF crystal is again

elucidated to be the close intermolecular S··S contacts greatly contributed by the inner sulfur atoms. In addition, the poor flatness of the C_1TET-TTF molecule would have increased a relative importance of the side-by-side interactions. In order to discuss the intermolecular interactions quantitatively, the intermolecular overlaps in these crystals should be investigated.

2-6. Donor Abilities of C_nTET-TTF in Solution

The redox properties of C_nTET-TTF in solution were investigated by cyclic voltammetry with a polarographic analyzer, Yanaco P-1100 and a X-Y recorder, GRAPHTEC WX2400. The potentials were measured in acetonitrile solutions at room temperature with respect to the saturated calomel electrode (SCE) by use of platinum electrodes as the working and counter electrodes. n-Bu_4NBF_4 was used as a supporting electrolyte (0.1 mol/dm^3 in acetonitrile).

The resulting values are summarized in Table 2-5 together with those of BEDT-TTF, TTC_1-TTF, and TTC_7-TTF measured in the same conditions. The first redox potential (E^1_{ro}) of C_nTET-TTF is independent of n within the experimental error indicating that the molecular ionization potential of C_nTET-TTF in solution is independent of the length of the alkyl chains (Fig. 2-16). The second redox potential (E^2_{ro}) and the difference (ΔE) between E^2_{ro} and E^1_{ro} of C_nTET-TTF are also independent of n (Table 2-5).

The redox potentials of C_nTET-TTF are almost equal to those of BEDT-TTF and TTC_n-TTF (Table 2-5). It is already known that TTC_nTTF shows constant redox potentials irrespective of n in solution[11]. These results indicate that the redox properties of the alkylated C_6S_8 electron donor in solution is not influenced by the shape and size of

the whole molecule. Such understandings would conform to the experimental result[28] that the ionization energy of BEDT-TTF and TTC_1-TTF is almost equal to each other in the gas phase, and to the calculated result[14a] that the electronic levels of the C_6S_8 core are scarcely influenced by its conformations.

Since the valence electronic states of C_nTET-TTF as one molecule can be regarded as insensible to the change of n, the n dependence of the resistivity in solid state (section 2-4) should come from the difference in the magnitude of interactions between the conjugation systems.

ΔE is considered to be a measure of the on-site Coulomb repulsive energy for a molecule. The value of C_nTET-TTF is comparable to that of BEDT-TTF which is known as a good electron donor giving a lot of conductive cation radical salts. Therefore, it is possible that C_nTET-TTF will give the conductive cation radical salts including superconductors, as far as its electronic property as one molecule is considered.

2-7. Summary

C_nTET-TTF (n=1, 2, 4, 7, 10, 13, 16, 18) was synthesized by the coupling reaction between the ketones. In spite of the large differences in the molecular shapes from TTC_n-TTF, C_nTET-TTF shows the n dependence of melting points similar to that of TTC_n-TTF, indicating an arrangement control of the C_6S_8 segments by two alkyl chains for a molecule in solid. This interpretation conforms to the result that the resistivity of C_{10}TET-TTF is smaller by a factor of four than that of C_2TET-TTF. C_1TET-TTF single crystals showed an extremely low resistivity (5.4×10^5 Ωcm) as a single component organic compound. The crystal structure analysis of C_1TET-TTF indicates that the C_6S_8 segment is bent in a boat form, and that several close sulfur to sulfur intermolecular contacts are observed in which the inner sulfur atoms greatly contribute to form the two-dimensional networks. The donor ability of C_nTET-TTF was measured by cyclic voltammetry. Its redox property in solution was independent of the length of alkyl chains, and almost equal to that of BEDT-TTF.

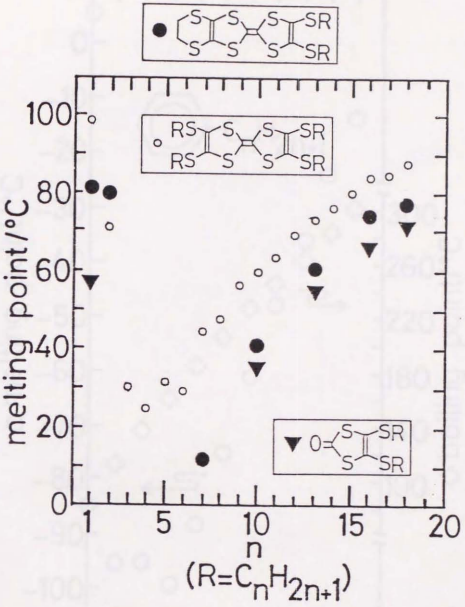

Fig. 2-1. Melting points of C_nTET-TTF and related compounds. The mp of C_4TET-TTF is lower than that (12 °C) of C_7TET-TTF. BEDT-TTF decomposes at 260 °C[15]. The data of TTC_n-TTF were reproduced from ref. 13a).

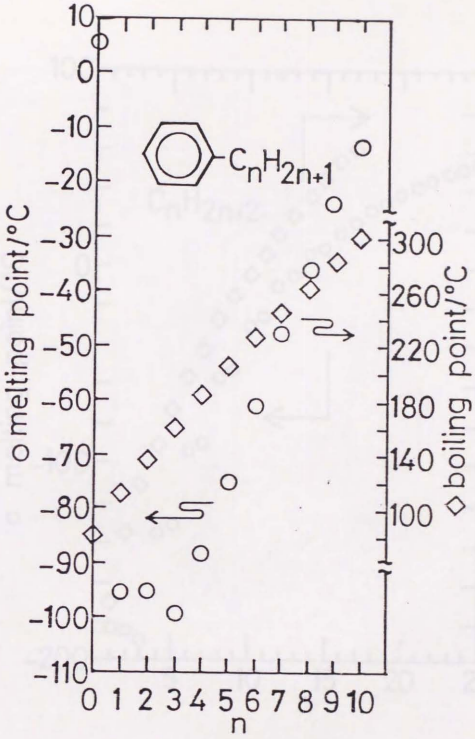

Fig. 2-2. Melting and boiling points of Ph-C_nH_{2n+1}.[68]

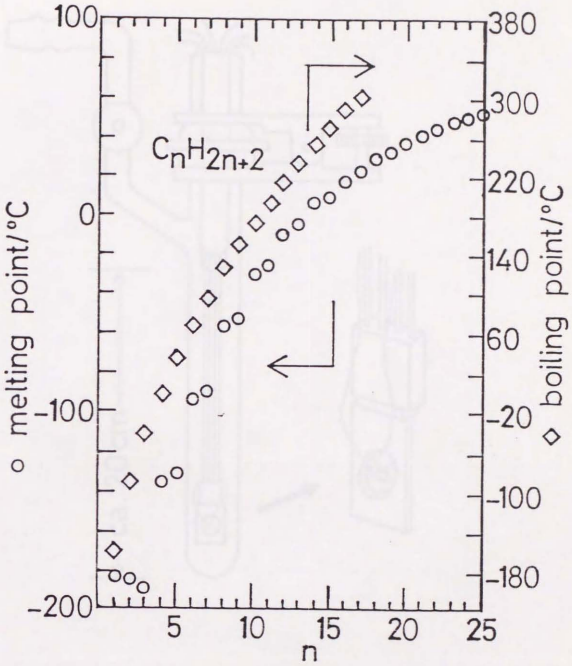

Fig. 2-3. Melting[69] and boiling[68] points of n-alkanes.

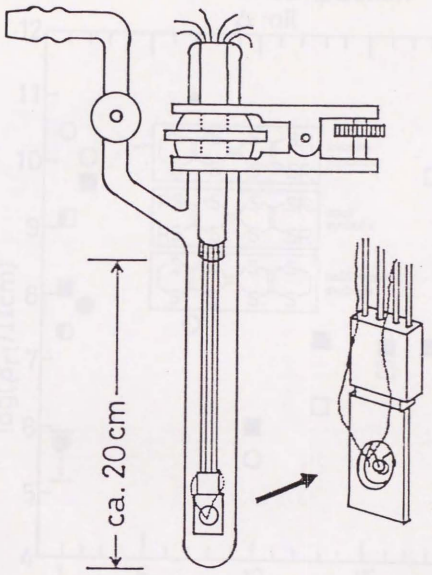

Fig. 2-4. The glass cell for the resistivity measurements.

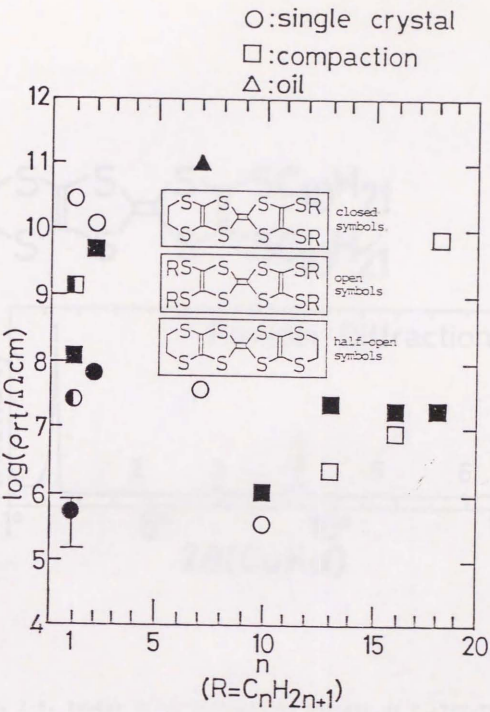

Fig. 2-5. Resistivities of C_nTET-TTF, TTC_n-TTF[12], and BEDT-TTF at room temperature.

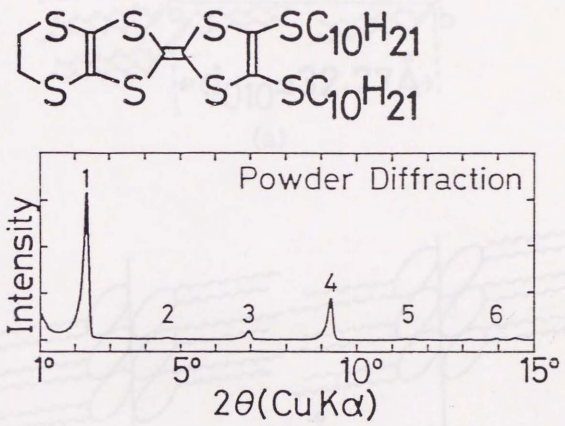

Fig. 2-6. Powder X-ray diffraction pattern of C_{10}TET-TTF. The numerals represent n in the equasion, $2d\sin\theta = n\lambda$, where d=38 Å and λ=1.542 Å.

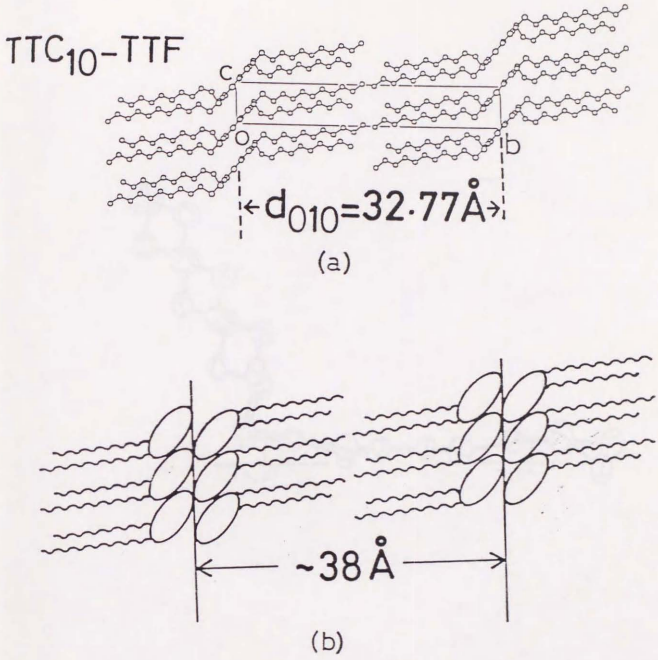

Fig. 2-7. (a) The crystal structure of TTC_{10}-TTF projected onto the bc plane[58]; (b) A schematic representation of the packing of C_{10}TET-TTF.

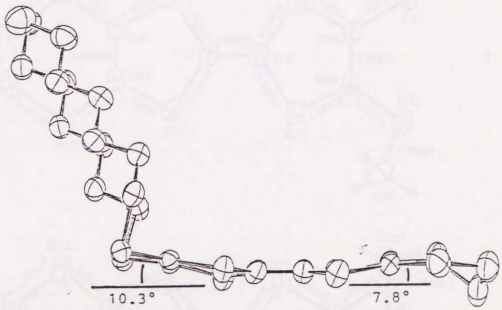

Fig. 2-8. The molecular side view of C_7TET-TTF in the crystal of (C_7TET-TTF)(TCNQ).

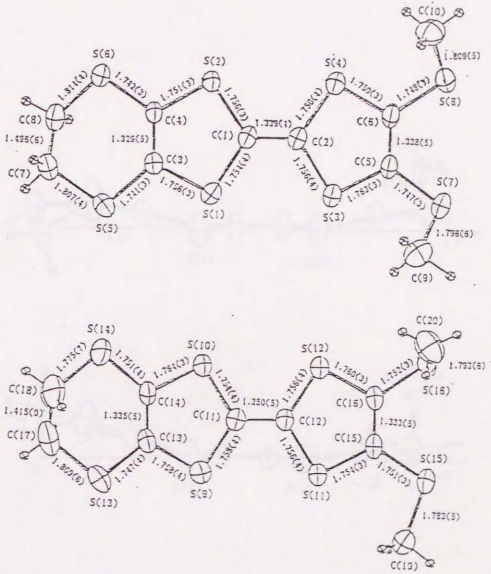

Fig. 2-9. Molecular structures of C_1TET-TTF.

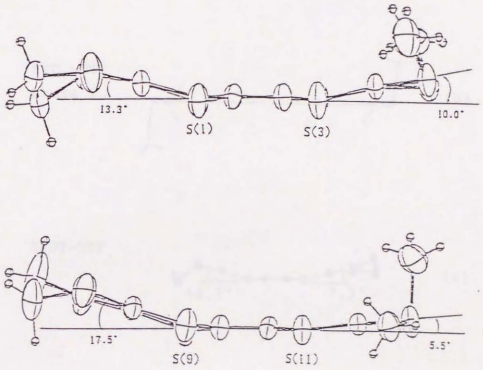

Fig. 2-10. Molecular side views of C_1TET-TTF.

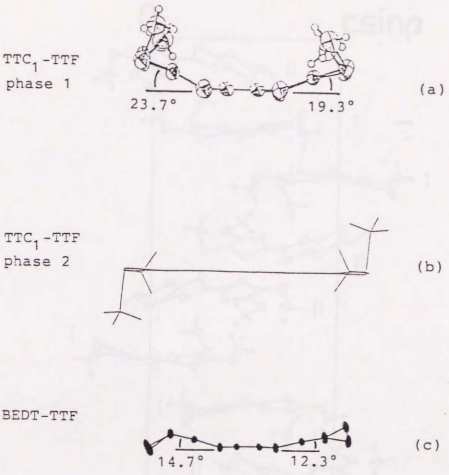

Fig. 2-11. Molecular side views of TTC_1-TTF (phase 1)[21a] (a), TTC_1-TTF (phase 2)[21b] (b), and BEDT-TTF[26] (c).

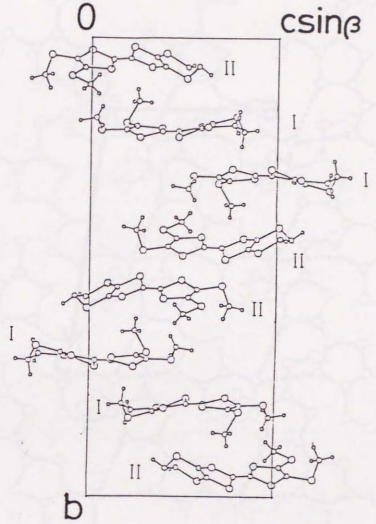

Fig. 2-12. Crystal structure of C_1TET-TTF projected along the a axis. I or II refers to the respective molecule in Figures 2-9 and 2-10.

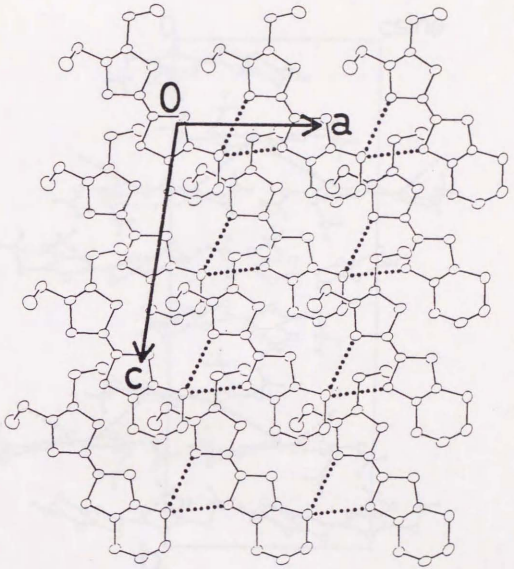

Fig. 2-13. The side-by-side arrangements of the molecule I along the a axis. The dotted lines indicate the close sulfur to sulfur distances (3.49~3.62 Å).

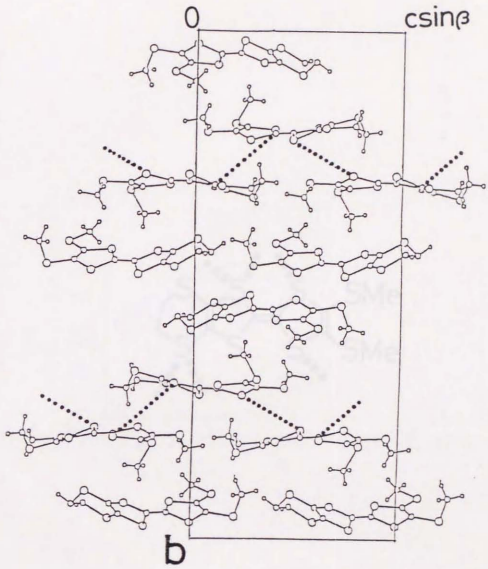

Fig. 2-14. The molecular arrangements along the c axis. The close sulfur to sulfur distances (3.60 Å) are only found among the molecules I.

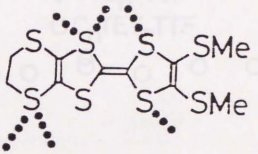

Fig. 2-15. The manner of the sulfur to sulfur interactions for a molecule I.

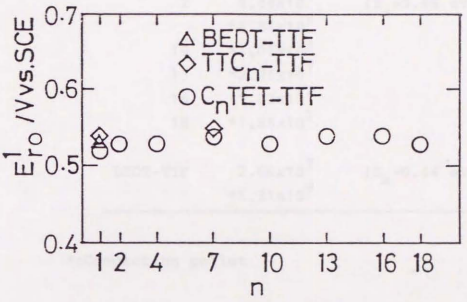

Fig. 2-16. The first redox potentials of C_nTET-TTF and the related molecules.
Pt vs. SCE in CH_3CN solution,
0.1 mol/dm^3 $TBABF_4$, 100 mV/s.

Table 2-1. Resistivities of C_nTET-TTF and BEDT-TTF.

n	$\rho_{rt}/\Omega cm$	
1	5.34×10^5	(E_a=0.26 eV)
	*1.17×10^8	
2	6.44×10^7	(E_a=0.45 eV)
	*4.81×10^9	
10	*1.01×10^5	
13	*2.26×10^7	
16	*1.83×10^7	
18	*1.85×10^7	
BEDT-TTF	2.60×10^7	(E_a=0.44 eV)
	*1.31×10^9	

*:Compaction pellet

Table 2-2. Crystallographic data for C_1TET-TTF.

Chemical Formula	$C_{10}H_{10}S_8$
FW	386.8
Crystal system	monoclinic
Space group	$P2_1/c$
a/Å	7.7821(9)
b	31.303(6)
c	13.021(1)
β/°	98.10(1)
V/Å^3	3140.4(7)
Z	8
d_{calcd}/gcm^{-3}	1.63
R	0.049
$2\theta_{max}$/°	60
No. of unique data ($\|F\| \geq 2\sigma(\|F\|)$)	6676
Crystal size/mm	0.35×0.35×0.30
(Mo Kα)/cm^{-1}	10.73
(Mo Kα)/Å	0.71069

Table 2-3. Atomic coordinates of C_1TET-TTF.

THE COORDINATES OF ATOMS (INPUT) AND THEIR STANDARD DEVIATIONS

NO	ATOM	X	Y	Z	AX	BY	CZ	S(X)	S(Y)	S(Z)
1	S1	1.04239	0.28496	0.97146	8.11198	8.92010	12.64938	0.00101	0.00125	0.00091
2	S2	0.76739	0.30715	1.09494	5.97190	9.61471	14.25722	0.00086	0.00125	0.00078
3	S3	0.76826	0.28439	0.76238	5.97868	8.90226	9.92695	0.00101	0.00125	0.00091
4	S4	0.48366	0.30388	0.88097	3.76389	9.51235	11.47111	0.00093	0.00125	0.00091
5	S5	1.33195	0.30702	1.13135	10.36537	9.61065	14.73130	0.00101	0.00157	0.00104
6	S6	1.01669	0.32935	1.28239	7.91178	10.30964	16.70451	0.00093	0.00125	0.00092
7	S7	0.54960	0.29953	0.55552	4.27704	9.37619	7.23343	0.00109	0.00125	0.00091
8	S8	0.22347	0.31557	0.69039	1.73907	9.87829	8.98957	0.00093	0.00125	0.00091
9	S9	0.74667	0.43632	0.82449	5.81066	13.65812	10.73568	0.00109	0.00125	0.00104
10	S10	1.01670	0.48088	0.72771	7.91206	15.05298	9.47551	0.00101	0.00125	0.00091
11	S11	0.50210	0.43261	0.60126	3.90739	13.54199	7.82901	0.00101	0.00125	0.00091
12	S12	0.77952	0.47311	0.50151	6.06630	14.80976	6.53016	0.00093	0.00094	0.00071
13	S13	0.97645	0.41191	1.01440	7.59883	12.89402	13.20850	0.00132	0.00157	0.00104
14	S14	1.29780	0.46591	0.90207	10.09961	14.58438	11.74585	0.00117	0.00125	0.00117
15	S15	0.27767	0.41714	0.39385	2.16086	13.05773	5.12832	0.00109	0.00125	0.00091
16	S16	0.58409	0.46167	0.28642	4.54545	14.45165	3.72947	0.00109	0.00125	0.00091
17	C1	0.82284	0.29782	0.97078	6.40342	9.32266	12.64053	0.00350	0.00407	0.00313
18	C2	0.70830	0.29708	0.88380	5.51206	9.29949	11.50796	0.00358	0.00407	0.00313
19	C3	1.10767	0.30437	1.09700	8.62000	9.54334	14.28404	0.00319	0.00376	0.00313
20	C4	0.98251	0.31471	1.15255	7.64599	9.85137	15.00735	0.00311	0.00344	0.00299
21	C5	0.57033	0.30111	0.69085	4.43836	9.42564	8.99556	0.00358	0.00407	0.00313
22	C6	0.44013	0.30894	0.74527	3.42513	9.67075	9.70416	0.00350	0.00376	0.00313
23	C7	1.36201	0.31149	1.27110	10.59930	9.75057	16.55098	0.00381	0.00470	0.00404
24	C8	1.20973	0.29747	1.32113	9.41424	9.31170	17.20242	0.00412	0.00438	0.00365
25	C9	0.74201	0.32662	0.52913	5.77439	10.22418	6.88980	0.00537	0.00657	0.00469
26	C10	0.16139	0.36272	0.75659	1.25595	11.35422	9.85156	0.00490	0.00470	0.00482
27	C11	0.81242	0.45616	0.70987	6.32233	14.27917	9.24322	0.00350	0.00407	0.00352
28	C12	0.71295	0.45388	0.61631	5.54825	14.20780	8.02497	0.00342	0.00376	0.00339
29	C13	0.95723	0.43760	0.89421	7.44926	13.69819	11.64351	0.00374	0.00407	0.00326
30	C14	1.07968	0.45797	0.85106	8.40218	14.33583	11.08165	0.00350	0.00376	0.00326
31	C15	0.47111	0.43547	0.46537	3.66622	13.63151	6.05958	0.00350	0.00376	0.00326
32	C16	0.59739	0.45311	0.42029	4.64895	14.18370	5.47260	0.00358	0.00376	0.00326
33	C17	1.17214	0.43707	1.07818	9.12171	13.68160	14.03899	0.00654	0.00720	0.00482
34	C18	1.31589	0.43876	1.02275	10.24039	13.73450	13.31723	0.00677	0.00876	0.00625
35	C19	0.15659	0.39940	0.49231	1.21860	12.50241	6.41037	0.00420	0.00501	0.00430
36	C20	0.71106	0.41806	0.24891	5.53354	13.08653	3.24106	0.00607	0.00595	0.00495
37	H7A	1.46150	0.29415	1.28922	11.37354	9.20778	16.78693	0.00000	0.00000	0.00000
38	H7B	1.39452	0.34110	1.29445	10.85229	10.67745	16.85503	0.00000	0.00000	0.00000
39	H8A	1.16563	0.26498	1.30820	9.07105	8.29467	17.03406	0.00000	0.00000	0.00000
40	H8B	1.23665	0.29962	1.38946	9.62374	9.37900	18.09213	0.00000	0.00000	0.00000
41	H9A	0.83600	0.30928	0.55679	6.50584	9.68139	7.24996	0.00000	0.00000	0.00000
42	H9B	0.72203	0.32229	0.44694	5.61891	10.08864	5.81960	0.00000	0.00000	0.00000
43	H9C	0.75815	0.35207	0.55983	5.90000	11.02084	7.28955	0.00000	0.00000	0.00000
44	H10A	0.16257	0.36057	0.82376	1.26514	11.28692	10.72618	0.00000	0.00000	0.00000
45	H10B	0.04234	0.36402	0.73057	0.32949	11.39491	9.51275	0.00000	0.00000	0.00000
46	H10C	0.22736	0.38601	0.74941	1.76934	12.08327	9.75807	0.00000	0.00000	0.00000
47	H17A	1.19659	0.41999	1.13595	9.31199	13.14694	14.79121	0.00000	0.00000	0.00000
48	H17B	1.12914	0.47350	1.07468	8.78708	14.82197	13.99341	0.00000	0.00000	0.00000
49	H18A	1.31290	0.40307	1.00679	10.21712	12.61730	13.10941	0.00000	0.00000	0.00000
50	H18B	1.43299	0.44200	1.05269	11.15167	13.83592	13.70707	0.00000	0.00000	0.00000
51	H19A	0.21882	0.37846	0.53581	1.70288	11.84693	6.97678	0.00000	0.00000	0.00000
52	H19B	0.05049	0.38896	0.45959	0.39292	12.17561	5.98432	0.00000	0.00000	0.00000
53	H19C	0.12961	0.41938	0.53810	1.00864	13.12785	7.00660	0.00000	0.00000	0.00000
54	H20A	0.67535	0.38995	0.27631	5.25564	12.20660	3.59783	0.00000	0.00000	0.00000
55	H20B	0.70628	0.41091	0.18125	5.49634	12.86271	2.36005	0.00000	0.00000	0.00000
56	H20C	0.82092	0.41749	0.28629	6.38848	13.06869	3.72778	0.00000	0.00000	0.00000

Table 2-4. The sulfur to sulfur interactions and the conducting properties of C_1TET-TTF, TTC_{10}-TTF, BEDT-TTF, and TTC_1-TTF (phase 1 and 2). *):This work

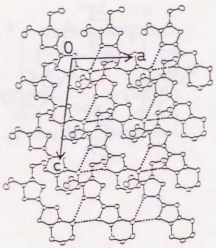

C_1TET-TTF*)

side-by-side 3.49∿3.62 Å

$\rho_{//a}=5.4\times10^5$ Ωcm (E_a=0.26 eV)

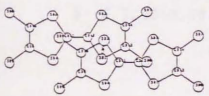

TTC_{10}-TTF

interplane 3.49 Å (S··S 3.57 Å)[58]

$\rho_{//stack}=3.7\times10^5$ Ωcm (E_a=0.13 eV)[12]

Table 2-4. (continued)

BEDT-TTF

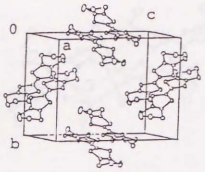

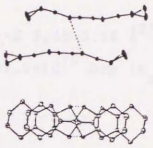

S··S 3.69 Å

26)

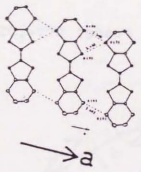

S··S 3.48∿3.69 Å[26)]

$\rho_{//a}=2.60\times10^{7}$ Ωcm (E_a=0.44 eV)*)

Table 2-4. (continued)

TTC_1-TTF (phase 1)

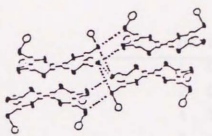

S··S 3.48∿3.66 Å[21a)]

$\rho=2.9\times10^{10}$ Ωcm (E_a=0.38 eV)[12)]

TTC_1-TTF (phase 2)[21b)]

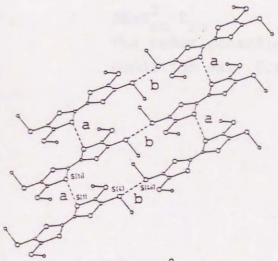

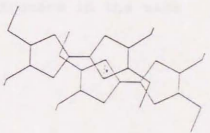

nearly flat molecular plane

a 3.72 Å

b 3.59 Å

Table 2-5. Redox potentials (V) of C_nTET-TTF and the related molecules.

Pt vs. SCE in CH_3CN solution,
0.1 mol/dm^3 $TBABF_4$, 100 mV/s.

	C_nTET-TTF		
n	E^1_{ro}	E^2_{ro}	ΔE
1	0.52	0.76	0.24
2	0.53	0.79	0.26
4	0.53	0.77	0.24
7	0.54	0.78	0.24
10	0.53	0.78	0.24
13	0.54	0.78	0.25
16	0.54	0.78	0.24
18	0.53	0.79	0.26
BEDT-TTF	0.53	0.77	0.24
TTC_1-TTF	0.54	0.77	0.23
TTC_7-TTF	0.55	0.79	0.24

$\Delta E = E^2_{ro} - E^1_{ro}$

The redox potential of ferrocene in the same condition was 0.44 V.

Table 2-6. Yields (%) and melting points of C_nTET-TTF.

n	%	m.p./°C
1	62	80.2-81.2
2	75	79.0-80.0
4	51	
7	58	11.4-13.4
10	70	40.5-41.0
13	37	61.0-62.0
16	52	73.0-74.0
18	43	76.5-77.5

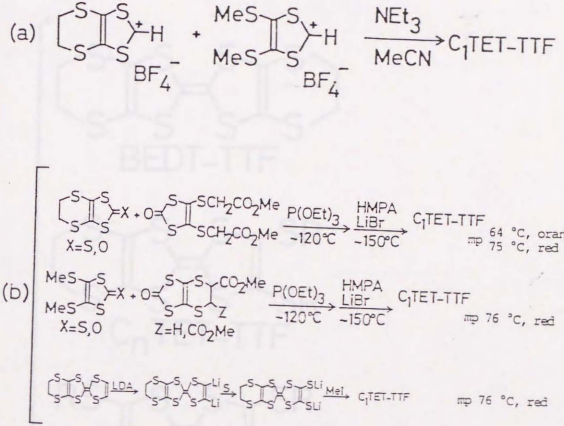

Scheme 2-1. Synthetic routes to C_1TET-TTF, (a)[29] and (b)[19].

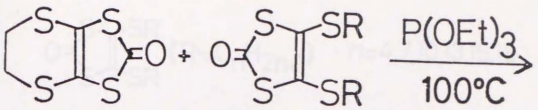

$R=C_nH_{2n+1}$

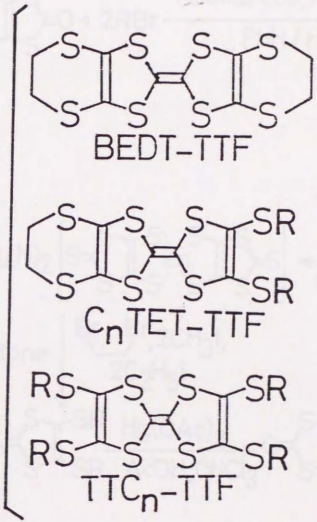

Scheme 2-2. Synthetic scheme of C_nTET-TTF.

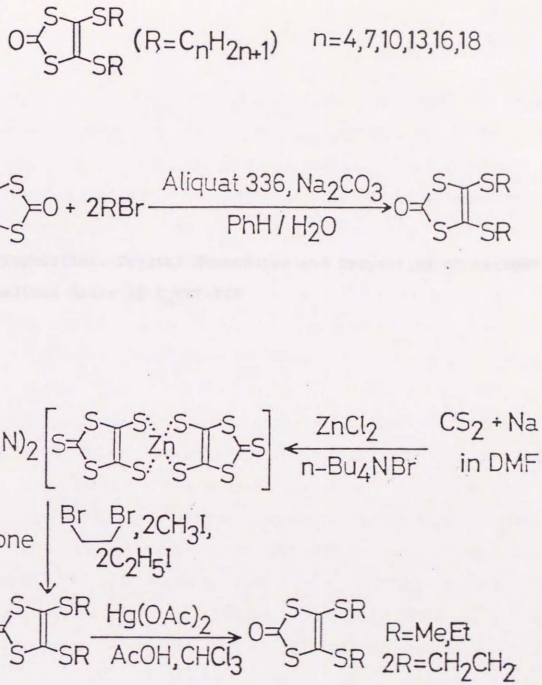

Scheme 2-3. Synthetic scheme of the ketones.

3. Preparation, Crystal Structures and Properties of Cation Radical Salts of C_nTET-TTF

3-1. Introduction

Among the C_6S_8 compounds in Fig. 1-1, BEDT-TTF has attracted the most attention because it has given a lot of metallic cation radical salts including superconductors. Its charge transfer (CT) complexes with organic acceptors have also been reported,[1), 35), 36)] but, the studies on single crystalline samples have been known only about (BEDT-TTF)(TCNQ).[36)] Contrary to the cation radical salts, a metallic conduction in BEDT-TTF CT complex has been observed only on the triclinic phase of (BEDT-TTF)(TCNQ) around room temperature.[36a)]

TTC_1-TTF has given more single crystalline CT complexes than BEDT-TTF has, probably due to its larger solubility in organic solvents. The single crystalline cation radical salts with inorganic anions have also been reported though they are inferior to those of BEDT-TTF in their kinds and numbers. TTC_1-TTF tends to give 1:1 salts with monovalent anions. As mentioned in section 1-2, $(TTC_1\text{-TTF})I_{2.47}$ is the only example in all TTC_1-TTF CT and radical complexes that shows the metallic temperature dependence of resistivity, so far.

Compared with the above two donors, TTC_n-TTF ($n \geq 2$) has scarcely been reported as a component of cation radical salts or CT complexes. A powder complex with the

composition of TTC_7-TTF:Br=1:6 was obtained by a direct mixing of TTC_7-TTF and bromine in hexane solution.[15] No other example of TTC_n-TTF ($n \geq 2$) complex with inorganic species is available in the literature. As for the CT complexes, TCNQ[37], F_4TCNQ[15], hexacyano-1,3-butadiene[15] (HCBD), 2,3-dibromo-5,6-dicyano-p-benzoquinone[15] (DBDQ), and 9-dicyanomethylene-2,4,5,7-tetranitrofluorene[27] (DTENF) were reported as acceptors. In the system of (TXC_n-TTF)(TCNQ) (X=S, Se, Te; n=2, 3), the structure analyses showed that the donor and acceptor molecules were alternately stacked in their crystals.[37] Imaeda et al. described that TXC_n-TTF ($n \geq 4$) did not form the CT complexes with TCNQ.[37]

According to our results,[15] TTC_7-TTF has more difficulty in forming CT complexes than C_7TET-TTF does. F_4TCNQ, HCBD, and DBDQ, which are all stronger acceptors than TCNQ, gave the complexes as solid with the both donors. TCNQ and more weaker acceptor, dimethyl TCNQ (DMTCNQ) formed the CT complexes with C_7TET-TTF but not with TTC_7-TTF. Although C_7TET-TTF has the alkyl chains only on its one side of the molecule, an aligning effect by the alkyl chains are recognized through the single crystal structure analyses[15), 38] on the neutral complexes, (C_7TET-TTF)(TCNQ) and (C_7TET-TTF)$_2$(DMTCNQ). It is desired to develop the cation radical slats of C_nTET-TTF, because the intrinsic character of the

unsymmetrical donor would be more clearly exhibited and more conductive substances would be expected than in its CT complexes, and because the arrangement of the radical part would be controlled by the alkyl chains which are directly attached to it.

Some related compounds to ours[15] possessing the long alkyl chains have been reported in connection with the formation of Langmuir-Blodgett films; C_nTET-TTF (n=12 and 18)[31], an unsymmetrical TTC$_n$-TTF[39], and BEDT-TTFC$_n$ (n=16, 18, and 20)[40].

The attempts to get the BEDT-TTF cation radical salts containing anionic surfactants as counter anions have been made but not succeeded.[15), 41]

Some of the complexes of C_1TET-TTF have appeared in the literature (TCNQ,[29] I_3,[19), 34] and IBr_2[19]), but the structures and physical properties of single crystals have not been described.

In this chapter, the cation radical salts of C_nTET-TTF are discussed especially on preparation, crystal structures, and conducting properties of C_1TET-TTF salts. An attention is also focused on $(C_1TET\text{-}TTF)_4Sb_2F_{11}$ which may result from the in situ generation of Sb_2F_{11} anion in the electrochemical process.

3-2. Preparation of Cation Radical Salts of C_nTET-TTF.

Since C_nTET-TTF shows the same redox properties as BEDT-TTF does in solution (section 2-6), we have tried preparing its cation radical salts by a conventional electrochemical method. The electron donor C_nTET-TTF (n=1, 2, 7, 13), and a supporting electrolyte n-Bu_4NX (X=PF_6, AsF_6, SbF_6, BF_4, ClO_4, ReO_4, I_3, IBr_2, AuI_2, $AuBr_2$, $Au(CN)_2$, Br_3, Br, I, CuSCN+KSCN+18-crown-6 ether, etc.) were dissolved in organic solvent (methanol, ethanol, acetonitrile, n-hexane, benzene, dichloromethane, etc.), and the electrolysis was carried out at a constant current (ca. 1 μA). A two-compartment H type glass cell and platinum electrodes were used (Fig. 3-1).

A typical procedure for the PF_6 salt of C_1TET-TTF was as follows. 5.6 mg of C_1TET-TTF (14.5 mmol) and 43.6 mg of $TBAPF_6$ (113 mmol) were place separately in the each compartment of the cell with Teflon coated stirring cores and the atmosphere in the cell was exchanged several times by argon gas. 18 cm^3 of dry methanol (distilled over magnesium methoxide) was added and the mixture was stirred under argon overnight. After the stirring cores were removed, the platinum rod electrodes of 1 mm in diameter and 4 cm long (burned just before the use) were immersed into both compartments through Teflon holders. The electrolysis

was carried out at a constant current of 1 μA at room temperature in the dark for 44 h. Black elongated plates were obtained, washed with methanol and dried under reduced pressure.

Up to now, the products have been obtained only from C_1TET-TTF and C_2TET-TTF. For n=7 or 13, the color of the solution changed from orange to dark brown as the current flowed, suggesting the formation of the cation radical of the donor. Any solid product was not crystallized, even when the electrolysis was carried out at ca. 5 °C for n=7. The reason why C_nTET-TTF of large n has difficulty in giving the salts may come from its long alkyl chains. The oxidation of the C_6S_8 segment may possibly influence the conformations of the alkylthio groups to restrict the directions of the alkyl chains. Further conditions of the solvents or temperature should be examined any way.

Table 3-1. summarizes the conducting properties of the cation radical salts of C_1TET-TTF and C_2TET-TTF obtained so far. Among them, those which show the metallic temperature dependence of resistivity will be described in sections 3-3 and 3-4.

3-3. $(C_1TET\text{-}TTF)_2{\sim}X$ (X=PF_6 and AsF_6)

3-3-1. Crystal Structures

We have determined the crystal structures of four kinds of C_1TET-TTF cation radical salts with respect to the anions (PF_6 or AsF_6) and solvents (methanol or ethanol) used.

X-Ray diffraction data for structure analyses of the PF_6 salts of C_1TET-TTF were collected at ambient temperature by an automated four-circle diffractometer, Enraf-Nonius CAD4, with graphite-monochromated Mo $K\alpha_1$ radiation (λ =0.70930 Å), using the 2θ-ω scan technique. Crystal structures were solved by a direct method using MULTAN82 program. A total of 3996 reflections were measured ($2° \leq 2\theta \leq 55°$) and 2053 reflections with $|F_o| \geq 2.5\sigma(|F_o|)$ were observed and 1962 independent ones were used for the analysis of the PF_6 salt grown in the methanol solution. A total of 4021 reflections were measured ($2° \leq 2\theta \leq 55°$) and 2072 reflections with $|F_o| \geq 3.0\sigma(|F_o|)$ were observed and 1987 independent ones were used for the analysis of the PF_6 salt grown in the ethanol solution. Non-hydrogen atoms were refined anisotropically including the occupancy of the anion using a full-matrix least-squares method. The final atomic parameters of the PF_6 salt grown in methanol and those of

the PF_6 salt grown in ethanol are listed in Tables 3-2 and 3-3, respectively.

X-Ray diffraction data for structure analyses of the AsF_6 salts of C_1TET-TTF were collected at room temperature by an automated four-circle diffractometer, Rigaku AFC-5, with graphite-monochromated Mo Kα radiation (λ=0.71069 Å), using the 2θ-ω scan technique. Crystal structures were solved by a direct method using MULTAN program. The structure of the AsF_6 salt of C_1TET-TTF grown in ethanol was refined anisotropically including the occupancy of the anion using 3018 independent reflections by a full-matrix least-squares method (RADIEL program).

Crystallographic data of the four crystals of C_1TET-TTF salts used for structure determination are summarized in Table 3-4. Only one crystallographically independent donor molecule is observed in each crystal.

The four PF_6 and AsF_6 crystals are isomorphic with slight differences in the anion arrangement (vide infra). The crystal structure of the PF_6 salt grown in methanol is shown in Fig. 3-2 as a representative. The donor molecules stack uniformly along the c axis which is the elongated direction of the crystal. The distance between the C_6S_3 planes in the column is 3.59 Å for the PF_6 salts, and 3.58 Å for the AsF_6 salts. No intermolecular sulfur to sulfur distance shorter than the sum of the van der Waals radii

(3.6∿3.7 Å) is observed within a column. The side view of a stacking column is shown in Fig. 3-3a. The mode of overlapping of the molecules within the column is shown in Fig. 3-3b. The molecules look to be slid diagonally each other so as to keep away from the methyl carbons possessing the large thermal motions.

On the other hand, some short S··S distances are found in the side-by-side direction (3.54∿3.68 Å for the PF_6 salts, and 3.54∿3.69 Å for the AsF_6 salts), and the donor molecules are slightly dimerized in that direction (Figures 3-4 and 3-5). These results present a contrast to those of β-(BEDT-TTF)$_2$$PF_6$[42] which has uniform and shorter side-by-side S··S contacts (3.44∿3.52 Å) and a tetrameric repeating unit in a column.

The projection along the long molecular axis is shown in Fig. 3-6. The regular spacing between the molecular planes and the short sulfur to sulfur distances in the side-by-side direction suggest a two-dimensional intermolecular interactions in the ac plane.

As shown in Figures 3-4 and 3-5, slight differences between the PF_6 salts and the AsF_6 salts are observed in the pattern of S··S contacts, though the mode of the shortest distances (3.54 Å) is common to each other. In the PF_6 salts, the short distances are observed only among the sulfur atoms of ethylenedithio groups and TTF skeletons

(Fig. 3-4). In the AsF_6 salts, one of the two sulfur atoms of the methylthio groups participates in the S··S networks (Fig. 3-5).

It is noteworthy that the asymmetric donor molecules are all oriented in the same direction within a column. It is hard to find such examples in the complexes of asymmetric TTF skeleton analogues except for (trimethylene-TTF)(TCNQ),[43] and $(MDT\text{-}TTF)_2Au(CN)_2$.[44] In the conventional complexes of noncentrosymmetric TTF analogues, the donor molecules stack alternately in head-to-tail manner within a column.[45), 46]

The interactions between hydrogen atoms and fluorine atoms are not recognized judging from the interatomic distances between the carbon atoms of the alkyl groups and the fluorine atoms.

The molecular structure of C_1TET-TTF in $(C_1TET\text{-}TTF)_2(AsF_6)_{0.79}$ with bond lengths is shown in Fig. 3-7 as a representative. The bendings of the C_6S_8 segment are decreased compared with the neutral molecules (Fig. 2-10). The ethylene group and the methyl groups are placed in the opposite side with respect to the molecular plane (Fig. 3-7b). The thermal motions of the ethylene carbons are large, indicating the conformational disorder. One of the methyl carbons are also disordered since it is observed in the two

positions. In the cation radical salts with partial charge transfer, the substitution of one ethylenedithio group of BEDT-TTF by two methylthio groups might cause the increase in freedom of the outer alkyl groups keeping the C_6S_8 core flat and rigid.

The bond lengths of the TTF skeletons in these cation radical salts are summarized in Table 3-5 together with those in the neutral C_1TET-TTF. According to the investigations on BEDT-TTF salts[47] and TTC_1-TTF salts[21a), 48)], the bond lengths of the TTF segment are sensitive to the change of the oxidation states of the molecule. However, any systematic correlation between the bond lengths and the formal charge of C_1TET-TTF can not be deduced from our result at present. The reason is not clear, and the other salts of C_1TET-TTF including those of 1:1 stoichiometry should be studied further.

Somewhat complicated anion arrangements were observed. In the PF_6 and AsF_6 salts grown in methanol, the anions are positionally disordered at two sites 0,0,1/2 and 0,0,0 with occupancies of 0.64 and 0.21 for the PF_6 salt, 0.61 and 0.18 for the AsF_6 salt, respectively. Thus the (D:X) of these salts are 2:0.85 and 2:0.79, respectively (see Table 3-4). Similar anion deficiencies were commonly recognized in other two salts grown in ethanol by structure refinements, and

were in some cases confirmed by elemental analyses and specific gravity measurements. In the salts grown in ethanol, the anion occupies 0,0,1/2 and shows no positional disorder. The occupancies of the anions are summarized in Table 3-6. One of the reasons for the deficiency and disorder of the anion would be the weak interaction between the anion and the alkyl groups of the donor (vide supra).

Satellite reflections with indices l=n±1/5 (n:integer) were clearly observed in oscillation photographs around the c axis at room temperature in the case of the PF_6 salt grown in methanol. These reflections indicate a fivefold modulation of the structure along the c axis. Similar superstructures were commonly observed in other three salts as temperature decreased. Such modulation would come from the anion deficiencies, the conformational disorders of the alkyl groups, and the positional disorders of the anions.

In our preliminary MS measurements on these salts grown in methanol or ethanol, a peak at m/e=32 or 46 was observed, respectively. The PF_6 salt grown in isopropanol gave a peak at m/e=60. Although it is possible to consider the incorporation of the solvent into the crystal accompanied by the anion deficiency, further investigations should be carried out to distinguish those peaks from many fragment peaks of C_1TET-TTF coexisting in such a low mass number region.

3-3-2. Conducting and EPR Properties

Electrical resistivity along the long axis of these crystals was measured by the standard d.c. four-probe method using 10 μm-diameter gold wires with gold paste (Tokuriki 8560) as electrical contacts, between room temperature and 1.5 K.

Electron paramagnetic resonance (EPR) spectra were recorded on an X-band spectrometer, JEOL JES-FE1XG with a cylindrical cavity (TE_{011}), equipped with a helium-flow cryostat, Air Products LTR-3-110. The single crystal was mounted on a quartz capillary with silicone grease, then sealed into a quartz sample tube with 10 mmHg pressure of helium gas. The temperature dependence of EPR spectra was measured for the static magnetic field normal to the long axis of the crystal and the g-factor maximum at room temperature. $Li^{+}TCNQ^{-}$ (g=2.0026) was used as a standard sample of g-factor. In some cases, the temperature dependence of the resistivity was measured for the same crystal that had been used for the EPR experiments after silicone grease was washed away with n-hexane.

The temperature dependence of common logarithm of conductivity for the four kinds of the C_1TET-TTF salts is shown in Fig 3-8. The data shown in Fig. 3-8 were obtained from the same crystals used for the EPR experiment (vide

infra). The room temperature conductivity was 10∿100 S/cm for each salt irrespective of the anion and solvent used (Fig. 3-8). In each case, the conductivity increased monotonically with decreasing temperature down to 150∿240 K. Such a metallic behavior is consistent with the crystal structures which indicate both the uniform overlap of the donor molecules along the stacking column and the partial charge transfer. Below the temperature at which the conductivity showed a maximum, the salts exhibited a semiconducting behavior. However, they did not obey the Arrhenius type activated manner in that low temperature region, indicating the invalidity of a simple semiconducting picture for these salts. At least 0.1 S/cm of conductivity was maintained in every case, even at 4.2 K.

For the PF_6 salts, somewhat temperature independent conductivity was often observed regardless of whether the solvent was methanol or ethanol (e.g. the PF_6 salt from methanol in Fig. 3-8). Since any other crystal modifications of these salts have not been detected at present, delicate differences in the degree of disorder seem to affect the transport properties in these crystals.

The anisotropy of the resistivity at room temperature in the largest crystal face of the PF_6 salt grown in methanol was about $\rho_{//c}:\rho_{\perp c}=1:10$. This observation supports the two-dimensional intermolecular interactions that the

crystal structure of this salt expects.

Figure 3-9 shows the angular dependence of g-factors and peak-to-peak linewidths (ΔH) for these crystals at room temperature. The crystals were rotated around the c axis. Only one Lorentzian signal was observed in the field range between 0 and 6500 G at room temperature for each crystal.

The angular dependence of g-factor for each crystal nearly coincides. This result suggests the nearly identical packings of the C_6S_8 cores in these crystals, as are already indicated by the X-ray structure determinations. The maximum (2.011) and minimum (2.005) g-factors were obtained when the static field was applied nearly parallel and normal to the a^* axis, respectively, and these values are comparable with the g-factors of BEDT-TTF cation radical salts.[56] Almost temperature independent g-factors were observed for each salts.

The salts grown in ethanol gave smaller linewidths than those grown in methanol (25 G vs. 28 G for PF_6, 22 G vs. 27 G for AsF_6 salts) at room temperature. This means that the relaxation of spins is faster in the salts obtained in methanol than in ones obtained in ethanol, and is consistent with the crystal structures which display the positional disorder of the anion only in the salts grown in methanol. A similar difference in linewidth related to the structural

disorder was reported for ß-(BEDT-TTF)$_2$I$_3$.[57]

Figure 3-10 shows relative intensity of EPR signal as a function of temperature for the four salts. These data had been collected before the data in Fig. 3-8 were obtained from the same crystals. In contrast to the somewhat various behaviors of conductivity (Fig. 3-8), normalized EPR intensity showed a common feature regardless of the anion or the solvent used (Fig. 3-10). It would be possible that the "contactless" measurement like EPR may be suited to extract the intrinsic properties of a crystal. In every case, the intensity gradually decreased bellow 200 K, and showed a minimum at around 50~60 K, then it increased at the lower temperature to reach the magnitude comparable to the room temperature value. No sudden decrease in the EPR intensity is observed in Fig. 3-10. The conductivity also decreases gently, as mentioned above. These situations rule out the existence of the phase transition at which the carriers disappear suddenly, in the investigated temperature range. The absolute magnitude of the spin susceptibility for the PF_6 salts was estimated to be about 4×10^{-4} emu/mol at 293 K.

Similar temperature-dependent spin susceptibility has been found in several organic "metals", for example, TTF-TCNQ[59], TTF-I_x[60], $(TTT)_2$-$I_{3+\delta}$[61], $(TMTTF)_2X$[62], and $(TMTSF)_2X$[63]. For those quasi-one-dimensional materials, it

has been considered that a pseudogap based on the one-dimensional fluctuation above the Peierls transition temperature can depress the density of states near the Fermi surface even in the metallic state.[64]

The Peierls pseudogap is unsuitable for the mechanism of the thermal variation of the susceptibility of the PF_6 and AsF_6 salts of C_1TET-TTF, because they are considered to be more two-dimensional on account of the structural and conducting properties mentioned previously. Another candidate to explain Fig. 3-10 above 50 K would be a mixture between the dimer model[65] and the Bonner-Fisher model[66], namely, the alternating antiferromagnetic chain model[67], but it is fundamentally for one-dimensional localized spins.

It is fruitful to remember that the PF_6 and AsF_6 salts of C_1TET-TTF exhibit the anion deficiency and the fivefold modulation of the structure along the stacking column (section 3-3-1). If the averaged stoichiometry is $(C_1TET\text{-}TTF)_2(X)_{0.8}$ (X=PF_6 or AsF_6), these salts should have a fifth-filled band. In this band filling, the fivefold periodic distortion of the lattice must produce a gap on a certain position of the Fermi surface, whether the Coulomb repulsion is strong or not. The gap formation like this will lead to a decrease in the density of states near the Fermi level as a whole, but will not mean the complete disappearance of the Fermi surface because these salts are

not one-dimensional. In fact, the PF_6 salt grown in methanol shows both a metallic conducting behavior and the fivefold satellite reflections simultaneously at around room temperature. The temperature-dependent spin susceptibility for these C_1TET-TTF salts above 50 K should come from the anisotropic fivefold modulation which would grow stronger at lower temperature.

The increase in the spin susceptibility below 50 K looks like a result of the superimposition of the Curie-like contribution on the conduction carrier paramagnetism, considering the moderate conductivity of these salts at 4.2 K. In order to estimate the concentration of the isolated spins at 4.2 K, we subtracted the conduction spin contribution from the measured susceptibility assuming the carrier concentration to be almost constant below 50 K. Then, the concentration of the isolated spins at 4.2 K for the PF_6 salt grown in methanol was estimated to be 10^{-3} spins/molecule. This result means that a spin is isolated on every thousand molecules on an average at the low temperature. The structural modulation along the molecular column and the complicated disorder must give such a concentration of the defects.

A random potential produced by the large magnitude of disorder in these C_1TET-TTF salts as well as a two dimensionality would be the reason why these salts do not

exhibit the metal to insulator phase transition.

3-4. $(C_1TET\text{-}TTF)_2X$ ($X=I_3$ or AuI_2)

The title salts were prepared by an electrochemical method essentially in the same way as described in section 3-3, except that $TBAI_3$ or $TBAAuI_2$ was used as a supporting electrolyte and acetonitrile as a solvent. Black hexagonal rods with luster from the I_3 anion, and black rhombic rods from the AuI_2 were obtained.

As for the crystals from I_3, X-ray photographs showed the presence of a superlattice structure characteristic of iodine complexes.[49] The structure determination of this salt has not succeeded, because the disorder exists at least in the two directions which is confirmed by oscillation and Weissenberg photographs along the crystal needle axis. The lattice constants were determined using a four-circle diffractometer (30 reflections, $30° \leq 2\theta \leq 40°$, MoKα): $a=11.60(1)$, $b=22.62(3)$, $c=9.65(4)$ Å, $\alpha=90.8(3)$, $\beta=97.2(3)$, $\gamma=89.7(1)°$, and $V=2512(11)$ Å^3. The ratio of the donor (D) to the anion regarded as I_3^- was estimated to be $D:I_3=1:\sim0.8$ by EPMA. These results reminiscent of $(TTC_1\text{-}TTF)I_{2.47}$ in which the iodine lattice composed of I_3^- columns is incommensurate with the donor lattice.[10]

The salt from AuI_2 gave the similar complicated oscillation photographs along the crystal needle axis. The ratio, $D:AuI_2$, was also estimated to be $1:\sim0.8$ by EPMA.

The two salts are referred to the I_3 salt and the AuI_2 salt, respectively for convenience.

Electrical resistivity and EPR spectra for the single crystals were measured essentially in the same way as described in section 3-3.

Figure 3-11 shows the temperature dependence of common logarithm of conductivity for the two salts. A metal to semiconductor transition was observed in the I_3 salt at 100 K, on the other hand, the AuI_2 salt showed a broad maximum of conductivity at around 250 K. The Arrhenius plots gave the activation energy, E_a=0.06 eV for the I_3 salt below 80 K, and E_a=0.05 eV for the AuI_2 salt below 130 K.

The EPR intensity of the I_3 salt starts to decrease from rather higher temperature than its transition in conductivity (Fig. 3-12a). The intensity is already decreased at 100 K to 30% of the room temperature value. Below 80 K, the signal behaves in an activated manner with E_a=0.03 eV.

The AuI_2 salt shows a somewhat constant intensity down to 220 K (Fig. 3-12b). The ln(IT) vs. T^{-1} plots shows a linear relation giving E_a=0.032 eV between 220 and 150 K (Fig 3-12c). Below 150 K, the data start to deviate from the line probably due to the Curie-like contribution.

3-5. $(C_1TET\text{-}TTF)_4Sb_2F_{11}$

3-5-1. Preparation and Properties

The sample was electrochemically prepared with a constant current of 0.8 $\mu A/cm^2$ in dry methanol solution of $C_1TET\text{-}TTF$ (1 $mmol/dm^3$) and $TBASbF_6$ (8 $mmol/dm^3$). In one or two weeks, black hexagonal rods (decomp.=195 °C) grew on the platinum anode.

The ratio of sulfur to antimony in this compound was estimated to be 16:1 by EPMA. The elemental analysis (found: C, 24.20; H, 2.14; N, 0; F, 10.20%) indicates that the composition of this product is $(C_1TET\text{-}TTF)_4Sb_2F_{11}$ (calcd: C, 24.03; H,2.02; F, 10.45%) and not $(C_1TET\text{-}TTF)_2SbF_6$ (calcd: C, 23.80; H, 2.00; F, 11.30%). As shown in 3-5-2, the structure determination exhibits that this product contains a binuclear anion of two antimony centered octahedra sharing a fluorine atom. In the IR spectra of this salt dispersed in a KBr pellet, the sharp and strong absorption was found at 640.4 cm^{-1} which was ascribed to the Sb-F stretching mode in comparison with $NF_4Sb_2F_{11}$[50a] and $TBASbF_6$. The absorption at 474.1 cm^{-1} was also observed but could not necessarily be assigned to the bending mode of the Sb-F-Sb bridge (480~497 cm^{-1})[50] because the absorption

ascribed to C_1TET-TTF was superimposed on that region.

In spite of the use of $TBASbF_6$ (its composition was confirmed by elemental analysis) as a supporting electrolyte, the electrochemical oxidation of C_1TET-TTF in methanol actually gave $(C_1TET\text{-}TTF)_4Sb_2F_{11}$ anyway. Usually, the Sb_2F_{11} anion is prepared in a strong acidic condition (e.g. $CsF+2SbF_5 \rightarrow CsSb_2F_{11}$, in SO_2[51]). In our case, the Sb_2F_{11} anion would be generated during the electrolysis and incorporated into the crystal, though the mechanisms are not clear at present. Similar unexpected in situ incorporation of fluorinated anions were recently observed in $(TMTSF)_3Ta_2F_{11}$[52] and probably in $(EOET\text{-}TTF)_2SbF_x$[53].

The absorption spectra of $(C_1TET\text{-}TTF)_4Sb_2F_{11}$ dispersed in a KBr pellet are shown in Fig. 3-13. The absorption was found at 4×10^3 and 11×10^3 cm^{-1}. The 4×10^3 cm^{-1} absorption could be ascribed to the CT transition between $C_1TET\text{-}TTF^{+}$s or that between $C_1TET\text{-}TTF^{+}$ and $C_1TET\text{-}TTF^{0}$. Since the 11×10^3 cm^{-1} absorption, which could be ascribed to one of the intramolecular transitions of $C_1TET\text{-}TTF^{+}$, somewhat broadens, another CT transition may superimpose on it.

The single crystal of this salt showed the conductivity of $\sigma_{rt}=0.4$ S/cm and the semiconducting behavior, $E_a=0.16$ eV (Fig. 3-14).

3-5-2. Crystal Structure

X-Ray diffraction data for structure analysis of $(C_1TET\text{-}TTF)_4Sb_2F_{11}$ were collected by an automated four-circle diffractometer, Rigaku AFC-5, with a graphite monochromated MoKα radiation, using the 2θ-ω scan technique. A total of 10125 reflections were measured ($3° \leq 2\theta \leq 60°$) and 6774 independent reflections were used for the analysis. The structure was solved by a direct method, and non-hydrogen atoms were refined anisotropically using a block-diagonal least-squares method. Crystallographic data are listed in Table 3-7, and the final atomic parameters are listed in Table 3-8, and F_o-F_c are listed in Table 3-10.

A noncentrosymmetric space group, P1 has been adopted for this crystal. The reduction in the symmetry of the model from $P\bar{1}$ to P1 gave a ten percent decrease in the R-value (0.069→0.062), and gave the Sb-F-Sb bridging angle of 155° which was consistent with the known value (vide infra). No satellite reflection was observed in oscillation and Weissenberg photographs at room temperature.

Crystallographically independent four donor molecules and one Sb_2F_{11} anion are contained in the unit cell (Fig. 3-15). The molecular structures of the donor are shown in Fig. 3-16 together with the numbering of atoms. No systematic difference was recognized in the bond lengths of

the four donor molecules. The thermal motions of the alkyl groups are relatively small (Table 3-9), and the strong interactions between the anion and the alkyl groups are observed (vide infra). This situation is in striking contrast to the PF_6 and AsF_6 salts in which the anion is also disordered. Such an interaction between the anion and alkyl groups must have a delicate effect upon the structure and physical properties of the salts.

The donor molecules stack almost in parallel to each other along the c axis which is the elongated direction of the crystal. The donors are oriented in the same direction within a stacking column (Fig. 3-17), similarly to the PF_6 and AsF_6 salts. A relatively short sulfur to sulfur distance (3.61 Å) was observed within the column to produce two kinds of overlaps in each column. The dimerization in a column is not serious, and the averaged distance between the C_6S_8 planes is 3.52 Å which is rather shorter than that of the PF_6 or AsF_6 salt (3.58∿3.59 Å).

In the transverse direction, the donors are seriously dimerized (Fig 3-18). The intermolecular sulfur to sulfur distances within the dimer are 3.38∿3.60 Å, and those between the dimers are 3.67∿3.70 Å.

The Sb_2F_{11} anion looks to assist the dimerization of the donors. The relatively short distances between the alkyl groups and the fluorine atom of the anion are observed

judging from vdW radii (Fig. 3-19). An extremely short C··F distance of 3.02 Å which is comparable to the sum of the vdW radii of carbon and fluorine (3.05 Å) suggests a hydrogen bond-like interaction.

The structure of the Sb_2F_{11} anion is shown in Fig. 3-20 together with the bond lengths. The coordination of Sb by F is octahedral with slight distortion. The averaged Sb-F length for each octahedron is 1.84 and 1.86 Å, as is usual[54]. The bridging Sb-F-Sb angle is 154.88(99)° in accord with the conventional value of 150~160°[55] for the angle at the μ-F atom of the $Sb_2F_{11}^-$ ion. Although the direct estimation of the valence of Sb in $(C_1TET\text{-}TTF)_4Sb_2F_{11}$ by ESCA was unsuccessful because of the decomposition of the sample, we could be able to regard the charge of Sb_2F_{11} in this salt as -1 on the basis of the structural data.

If no charge separation exists among the donor molecules, the charge of the one donor is +0.25 meaning a partial charge transfer. However, this salt is a semiconductor as mentioned above. The strong distortion in the donor packing of this salt would be responsible for the semiconducting property.

3-6. Salts of C_2TET-TTF

The PF_6 salt and the ClO_4 salt of C_2TET-TTF were obtained as black elongated plates by the electrochemical method. The compositions and crystal structures of these salts have not been determined yet. The resistivity of these single crystals were measured by the four-probe method. Both salts showed the room temperature conductivity of 10 S/cm. As shown in Fig. 3-21, each salt exhibited the metallic temperature dependence down to about 60 K for the PF_6 salt and about 80 K for the ClO_4 salt. The activation energy just below the transition was estimated to be 0.08, and 0.14 eV, respectively. The clear metal to semiconductor transitions in these salts present a striking contrast to the PF_6 and AsF_6 salts of C_1TET-TTF.

3-7. Summary

In this chapter, the cation radical salts of C_nTET-TTF were treated especially focusing on the C_1TET-TTF salts. The PF_6 and AsF_6 salts of C_1TET-TTF were isomorphic with characteristic anion deficiency. They showed the metallic temperature dependence of resistivity at least down to 240 K. Some kind of superlattice was observed in every C_1TET-TTF salt structurally investigated, except for the Sb_2F_{11} salt. The side-by-side intermolecular interactions were recognized in these cation radical salts, similarly to the neutral C_1TET-TTF crystal. The interactions between the anion and the alkyl groups of the donor must influence the structure and physical properties of the salts. The appearance of the anion deficiency in the C_1TET-TTF salts may indicate the flexibility of this donor molecule in its electronic states as well as in its structural aspects. If we could control the oxidation states of the donor molecule in solid state for example by the anion deficiency, we would be able to touch the band filling.

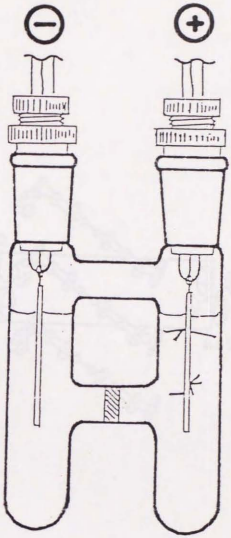

Fig. 3-1. A two-compartment glass H-cell for elctrolysis.

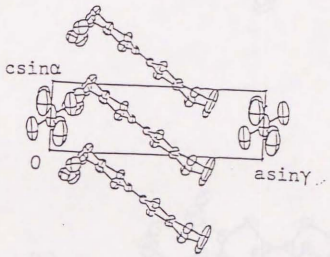

Fig. 3-2. Crystal structure of $(C_1TET\text{-}TTF)_2(PF_6)_{0.85}$ grown in methanol projected along the b axis. The anion at 0,0,0, is omitted.

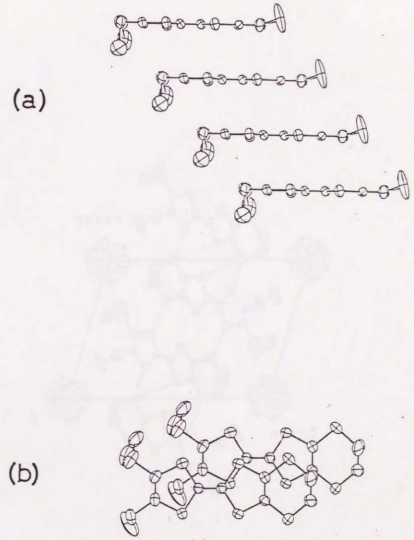

Fig. 3-3. (a) Side view of a stacking column of the donor molecules in $(C_1TET\text{-}TTF)_2(PF_6)_{0.85}$; (b) Mode of overlaps of $C_1TET\text{-}TTF$ within the column.

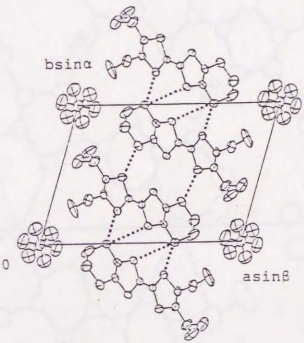

Fig. 3-4. Crystal structure of $(C_1TET\text{-}TTF)_2(PF_6)_{0.85}$ projected along the c axis. The dotted lines show short sulfur to sulfur distances (3.54∿ 3.68 Å).

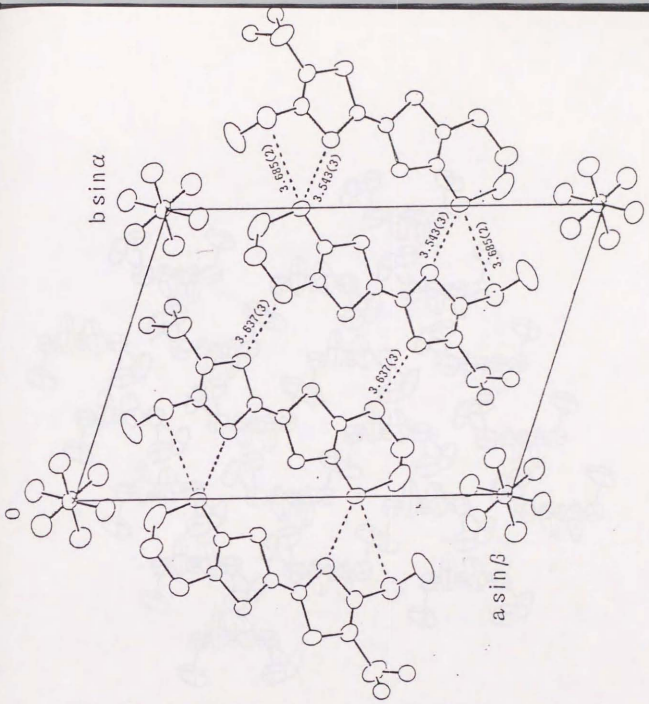

Fig. 3-5. Crystal structure of $(C_1TET\text{-}TTF)_2(AsF_6)_{0.79}$ projected along the c axis. The dotted lines show short sulfur to sulfur distances (3.54∿ 3.69 Å).

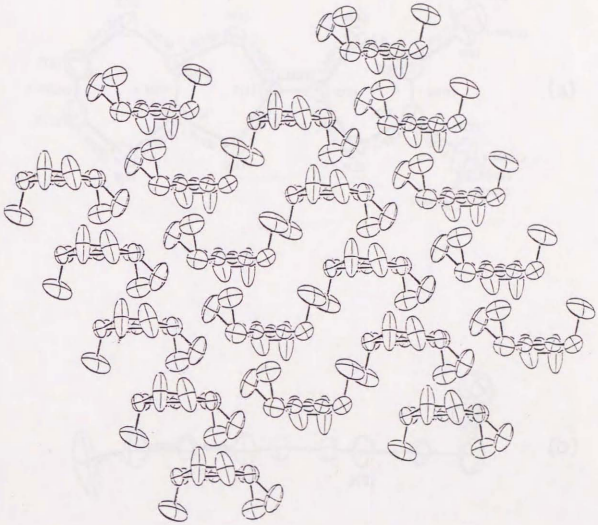

Fig. 3-6. Molecular arrangement in $(C_1TET\text{-}TTF)_2(PF_6)_{0.85}$ projected along the long molecular axis of the donor.

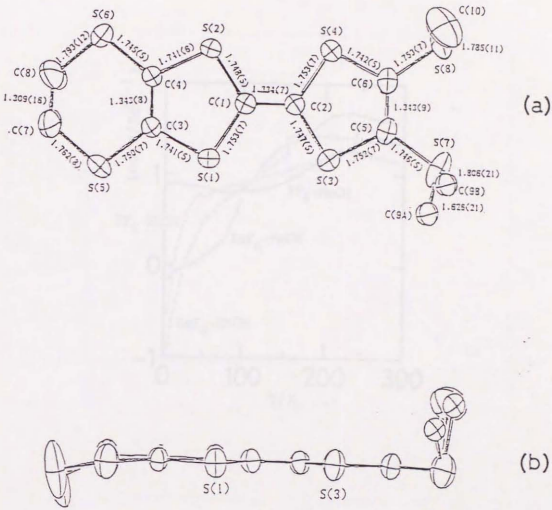

Fig. 3-7. Molecular structure of C_1TET-TTF in $(C_1\text{TET-TTF})_2(AsF_6)_{0.79}$, (a) top view; (b) side view.

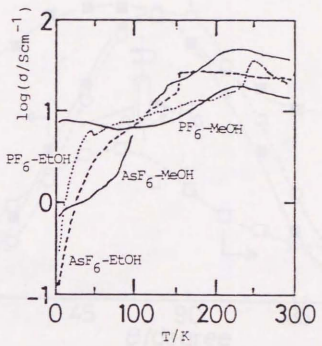

Fig. 3-8. The temperature dependence of common logarithm of conductivity of the four C_1TET-TTF salts for the same crystals used in the EPR experiments (Fig. 3-10).

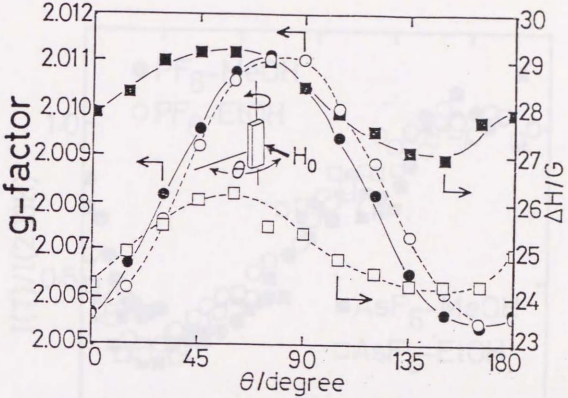

Fig. 3-9. Angular dependence of g-factors and peak-to-peak linewidths (ΔH) of the C_1TET-TTF salts of PF_6 at room temperature. Closed symbols are for a crystal grown in methanol, open ones are for a crystal grown in ethanol. The lines drawn are visual guides.

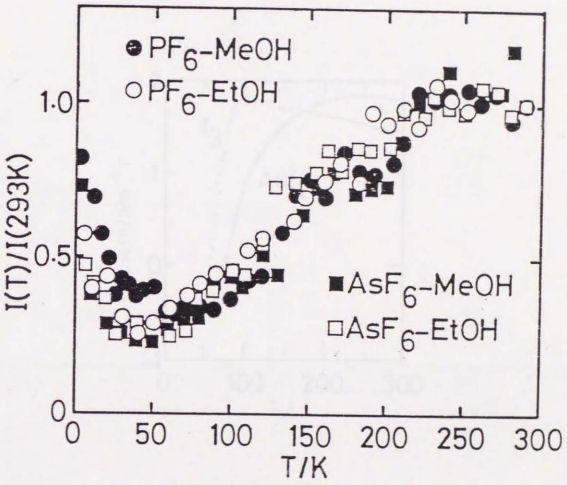

Fig. 3-10. The temperature dependence of relative EPR intensity of the four C_1TET-TTF salts. The spin susceptibility of the PF_6 salt grown in methanol was about 4×10^{-4} emu/mol at 293 K.

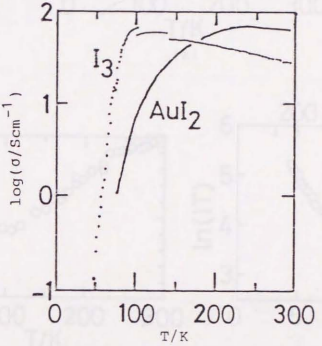

Fig. 3-11. The temperature dependence of common logarithm of conductivity of the I_3 and AuI_2 salts of C_1TET-TTF.

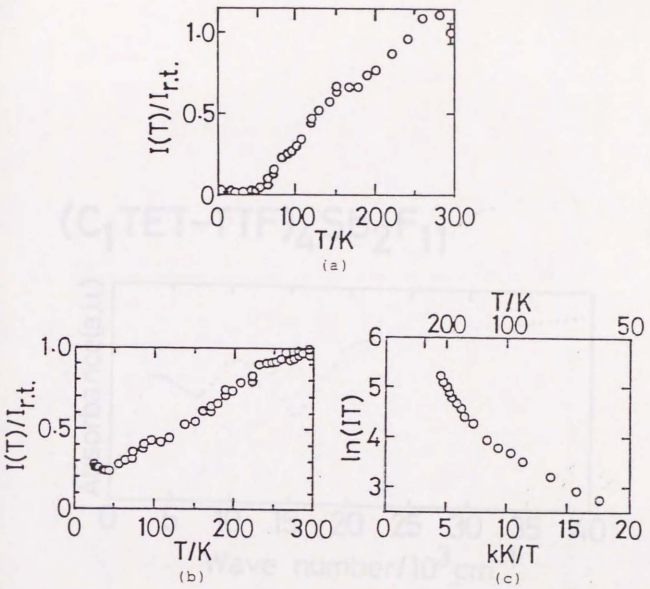

Fig. 3-12. (a) The temperature dependence of relative EPR intensity of the I_3 salt of C_1TET-TTF; (b) The temperature dependence of relative EPR intensity of the AuI_2 salt of C_1TET-TTF; (c) ln(IT) vs. 1/T plots for the AuI_2 salt of C_1TET-TTF.

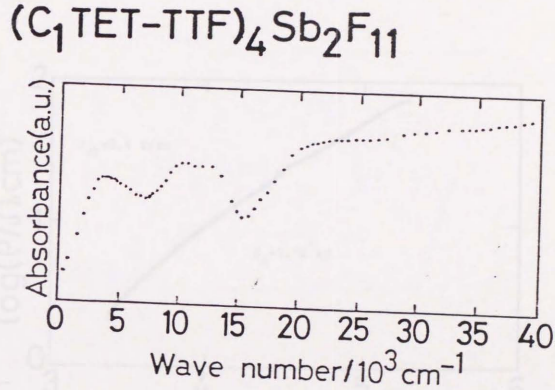

Fig. 3-13. The absorption spectra of $(C_1TET\text{-}TTF)_4Sb_2F_{11}$ at room temperature (KBr pellet).

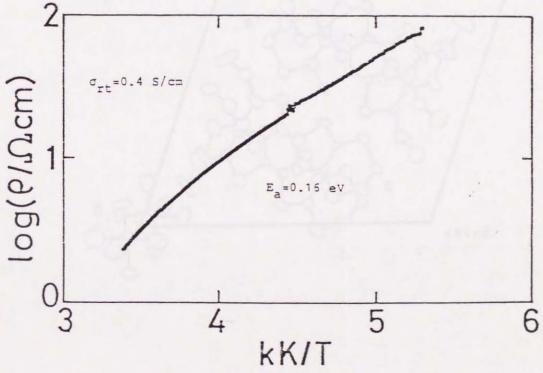

Fig. 3-14. lg(ρ/Ωcm) vs. 1/T plots for $(C_1TET\text{-}TTF)_4Sb_2F_{11}$ measured by the four-probe method with gold paste as contacts.

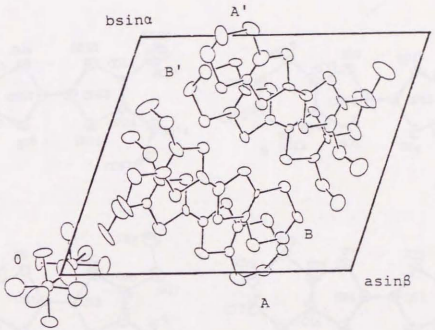

Fig. 3-15. The crystal structure of $(C_1TET\text{-}TTF)_4Sb_2F_{11}$ projected along the c axis. A, A', B, or B' represents the independent molecule, respectively.

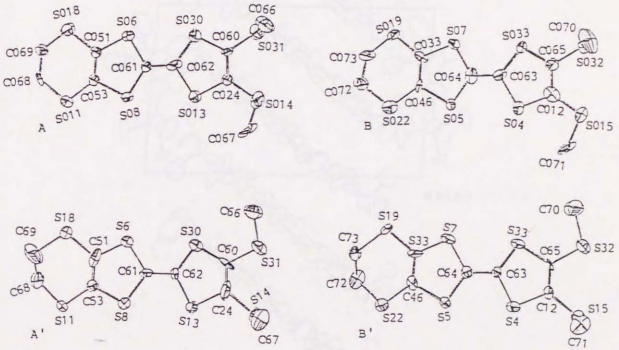

Fig. 3-16. Molecular structures of the four donors in $(C_1TET\text{-}TTF)_4Sb_2F_{11}$.

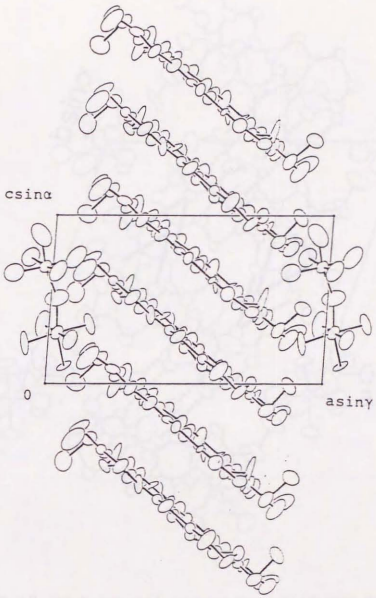

Fig. 3-17. The crystal structure of $(C_1TET\text{-}TTF)_4Sb_2F_{11}$ projected along the b axis.

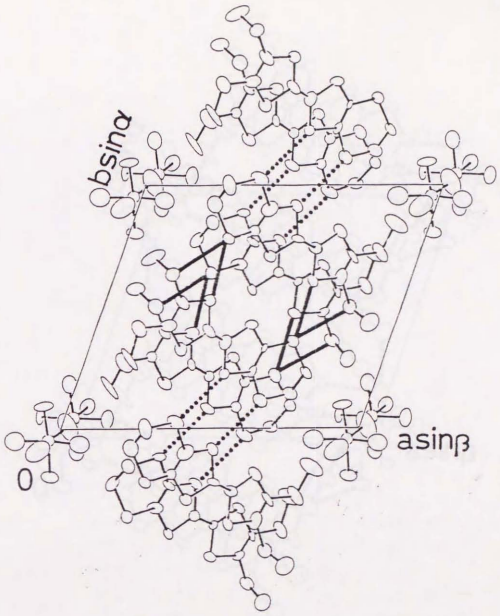

Fig. 3-18. The crystal structure of $(C_1TET\text{-}TTF)_4Sb_2F_{11}$ projected along the c axis. The solid and dotted lines show the sulfur to sulfur distances of 3.38∿3.60 Å and 3.67∿3.70 Å, respectively.

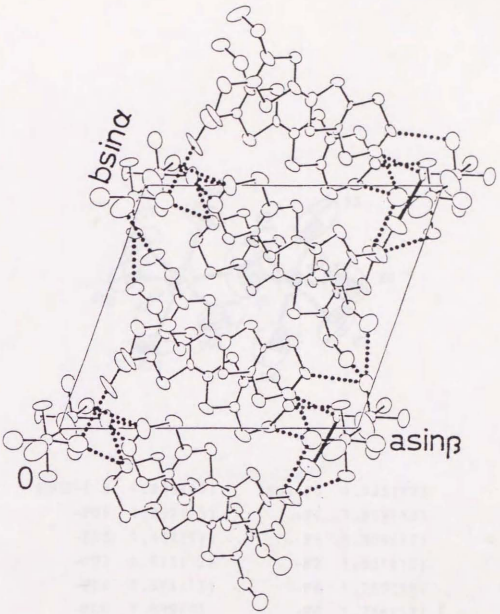

Fig. 3-19. The contacts between the fluorine atoms of the anion and the carbon atoms of alkyl groups. The solid and dotted lines show carbon to fluorine distances of 3.02 Å and 3.12∿3.34 Å, respectively.

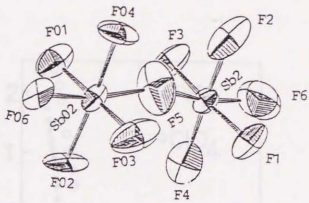

Sb02-F 5	1.830(17)	Sb2-F5	1.925(17)
-F01	1.832(13)	-F1	1.899(12)
-F03	1.842(17)	-F3	1.906(12)
-F02	1.873(12)	-F2	1.821(15)
-F04	1.894(13)	-F4	1.759(15)
-F06	1.879(9)	-F6	1.728(17) Å

Fig. 3-20. The structure of the Sb_2F_{11} anion in $(C_1TET\text{-}TTF)_4Sb_2F_{11}$.

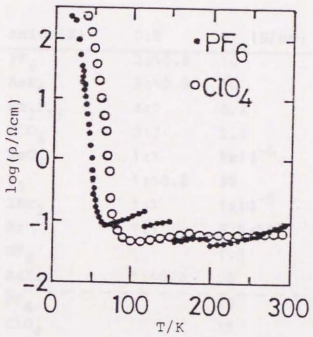

Fig. 3-21. The temperature dependence of resistivity of the PF_6 and ClO_4 salts of C_2TET-TTF.

Table 3-1. The conducting properties of C_nTET-TTF (n=1 and 2) salts. The resistivities were measured by the four probe method with gold paste as contacts except that the ReO_4, IBr_2, and Br salts were measured by the two probe method. T_{min} refers to the temperature at which the resistivity comes to the minimum. The composition (D:X) is the value estimated by EPMA.

n	anion(X)	D:X	σ_{rt}(S/cm)	
	PF_6	2:∿0.8	10	metallic
	AsF_6	2:∿0.8	10	metallic
	Sb_2F_{11}	4:1	0.4	E_a=0.16 eV
	ClO_4	3:2	2.5	E_a=0.09 eV
1	ReO_4	1:1	9×10^{-6}	E_a=0.21 eV
	I_3	1:∿0.8	30	T_{min}=100 K
	IBr_2	1:1	1×10^{-5}	E_a=0.20 eV
	Br	1:1	6.5×10^{-3}	E_a=0.15 eV
	BF_4		1.5	E_a=0.63 eV
	AuI_2	1:∿0.8	60	T_{min}=250 K
2	PF_6		10	T_{min}=60 K
	ClO_4		15	T_{min}=80 K

Table 3-2. Atomic parameters of $(C_1TET\text{-}TTF)_2(PF_6)_{0.85}$ grown in methanol.

$B=(4/3)\Sigma\Sigma B_{ij}a_i a_j$
$\quad\quad ij$

N	ATOM	X	Y	Z	B	ISF	AI
1	P1	0.0	0.0	0.5000	10.89	2	0.32
2	P2	0.0	0.0	0.0	9.05	2	0.10
3	F1	-0.0869	0.0290	0.2970	13.96	3	0.85
4	F2	0.0439	-0.1168	0.2462	16.58	3	0.85
5	F3	0.0411	0.0800	0.3007	16.10	3	0.85
6	S1	0.4923	0.3698	0.1734	3.95	1	1.00
7	S2	0.5129	0.1239	0.2926	3.91	1	1.00
8	S3	0.6480	0.2541	-0.1962	5.01	1	1.00
9	S4	0.6708	0.0013	-0.0578	4.48	1	1.00
10	S5	0.3161	0.4775	0.5596	4.48	1	1.00
11	S6	0.3399	0.2328	0.6928	3.82	1	1.00
12	S7	0.1555	0.5973	0.9209	7.55	1	1.00

N	ATOM	X	Y	Z	B	ISF	AI
13	S8	0.1799	0.3146	1.0625	5.59	1	1.00
14	C1	0.5802	0.2487	0.0105	3.26	4	1.00
15	C2	0.5902	0.1381	0.0634	3.25	4	1.00
16	C3	0.7418	0.1580	-0.2484	10.05	4	1.00
17	C4	0.7512	0.0563	-0.1959	11.85	4	1.00
18	C5	0.2383	0.4624	0.7901	4.06	4	1.00
19	C6	0.2481	0.3539	0.8461	3.83	4	1.00
20	C7A	0.0742	0.6042	0.6661	7.56	4	0.46
21	C7B	0.1169	0.6746	0.6572	10.34	4	0.54
22	C8	0.1123	0.2514	0.3021	9.02	4	1.00
23	C9	0.4507	0.2777	0.3484	3.36	4	1.00
24	C10	0.3787	0.3219	0.5094	3.36	4	1.00

Table 3-3. Atomic parameters of $(C_1TET\text{-}TTF)_2(PF_6)_{0.94}$ grown in ethanol.

$$B=(4/3)\sum\sum_{ij} B_{ij} a_i a_j$$

N	ATOM	X	Y	Z	B	ISF	AI
1	P1	0.0	0.0	0.5000	5.84	2	0.47
2	F1	-0.0882	0.0291	0.3237	7.69	3	0.94
3	F2	0.0440	-0.1186	0.2749	7.78	3	0.94
4	F3	0.0394	0.0808	0.3355	8.05	3	0.94
5	S1	0.4914	0.3715	0.1791	3.29	1	1.00
6	S2	0.5121	0.1240	0.2930	3.22	1	1.00
7	S3	0.6463	0.2978	-0.1944	4.30	1	1.00
8	S4	0.6703	0.0025	-0.0620	3.92	1	1.00
9	S5	0.3160	0.4774	0.5731	3.70	1	1.00
10	S6	0.3419	0.2313	0.7024	3.32	1	1.00
11	S7	0.1554	0.5931	0.9408	6.24	1	1.00
12	S8	0.1837	0.3118	1.0835	4.54	1	1.00

N	ATOM	X	Y	Z	B	ISF	AI
13	C1	0.5786	0.2500	0.0111	2.69	4	1.00
14	C2	0.5888	0.1395	0.0632	2.63	4	1.00
15	C3	0.7372	0.1581	-0.2235	7.79	4	1.00
16	C4	0.7551	0.0618	-0.1619	8.62	4	1.00
17	C5	0.2380	0.4600	0.8006	3.32	4	1.00
18	C6	0.2512	0.3514	0.8601	2.96	4	1.00
19	C7A	0.0734	0.6007	0.6714	7.43	4	0.45
20	C7B	0.1251	0.6765	0.6916	6.75	4	0.55
21	C8	0.1155	0.2479	0.8412	7.64	4	1.00
22	C9	0.4508	0.2776	0.3447	2.56	4	1.00
23	C10	0.3780	0.3227	0.5155	2.62	4	1.00

Table 3-4. Crystallographic data of the C_1TET-TTF salts at room temperature.

anion	PF_6		AsF_6	
solvent used	MeOH	EtOH	MeOH	EtOH
space group	$P\bar{1}$	$P\bar{1}$	$P\bar{1}$	$P\bar{1}$
a/Å	15.859(4)	15.768(3)	15.980(2)	15.948(2)
b	11.601(4)	11.563(1)	11.625(2)	11.587(2)
c	4.880(5)	4.938(1)	4.8893(8)	4.9262(10)
α/°	100.12(5)	100.14(1)	99.94(2)	99.90(2)
β	92.53(5)	92.24(2)	92.39(2)	92.16(2)
γ	72.51(2)	72.70(1)	72.68(1)	72.74(1)
$V/Å^3$	843(1)	846(3)	854.1(2)	856.3(3)
d_{calc}/gcm^{-3}	1.77	1.79	1.79	1.79
d_{obs}/gcm^{-3}	1.76			1.83
R	0.073	0.072	0.079	0.064
Z	1	1	1	1
D:X	2:0.85	2:0.94	2:0.79	2:0.79

Table 3-5. Bond lengths of C_1TET-TTF. The bond lengths are averaged by assuming C_{2v} symmetry.

compound	bond length/Å						
	1	2	3	4	5	6	7
neutral molecule I	1.339(4)	1.329(5)	1.338(5)	1.755	1.756	1.734	1.761
neutral molecule II	1.350(5)	1.335(5)	1.333(5)	1.756	1.756	1.761	1.757
$(C_1TET\text{-}TTF)_2(AsF_6)_{0.79}$	1.334(7)	1.343(8)	1.343(9)	1.751	1.750	1.741	1.747
$(C_1TET\text{-}TTF)_2(PF_6)_{0.85}$	1.331(14)	1.314(16)	1.297(17)	1.750	1.746	1.756	1.773
$(C_1TET\text{-}TTF)_2(PF_6)_{0.94}$	1.366(12)	1.309(14)	1.295(15)	1.741	1.742	1.752	1.768

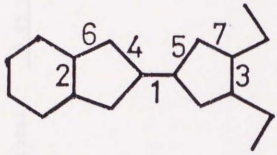

Table 3-6. The occupancies of the anions in the C_1TET-TTF salts.

	occupancies			
	MeOH		EtOH	
site	PF_6	AsF_6	PF_6	AsF_6
0,0,1/2	0.64	0.61	0.94	0.79
0,0,0	0.21	0.18	0	0
total	0.85	0.79	0.94	0.79

Table 3-7. Crystallographic data of $(C_1TET\text{-}TTF)_4Sb_2F_{11}$.

Chemical Formula	$C_{40}H_{40}S_{32}Sb_2F_{11}$
FW	1999.35
D:X	4:1
Crystal system	triclinic
Space group	P1
a/Å	15.645(5)
b	13.396(4)
c	8.943(2)
α/°	81.95(2)
β/	83.45(3)
γ/	69.43(2)
V/Å^3	1733(1)
Z	1
d_{calcd}/gcm^{-3}	1.914
d_{obs}/gcm^{-3}	1.94
R	0.062

Table 3-8. Atomic parameters of $(C_1TET\text{-}TTF)_4Sb_2F_{11}$.

NO	ATOM	X	Y	Z	B11 OR B	B22	B33	B12	B13	B23	G	ITBL
1	F 5	0.02074	0.01065	0.51041	0.015125	0.026383	0.018499	-0.013876	0.002841	0.000275	1.000	3
2	SB02	0.02900	0.04654	0.30545	0.003999	0.005761	0.013490	-0.002017	0.002203	-0.002985	1.000	1
3	F 04	-0.08440	0.05325	0.24150	0.001904	0.008823	0.043524	-0.002225	-0.004052	-0.005746	1.000	3
4	F 03	-0.02337	0.18550	0.35352	0.005479	0.011110	0.053391	-0.003431	0.003033	-0.011585	1.000	3
5	F 01	0.07847	-0.09261	0.26092	0.005877	0.010281	0.028366	-0.003408	0.003770	-0.006813	1.000	3
6	F 02	0.14420	0.03953	0.35533	0.003988	0.012240	0.032569	-0.002717	-0.006410	-0.002139	1.000	3
7	F 06	0.06281	0.09307	0.10682	0.005711	0.009059	0.007227	-0.001435	0.004434	0.004606	1.000	3
8	SB 2	-0.02854	-0.04571	0.69677	0.003722	0.005058	0.010458	-0.001499	0.001328	-0.000454	1.000	1
9	F 4	0.08015	-0.06163	0.75240	0.010060	0.010099	0.035329	-0.003511	0.008019	-0.007800	1.000	3
10	F 3	0.01890	-0.19445	0.66974	0.007980	0.004768	0.031714	-0.002198	0.006550	-0.005836	1.000	3
11	F 1	-0.08401	0.09586	0.75249	0.008519	0.003001	0.026180	0.000367	0.002745	-0.004996	1.000	3
12	F 2	-0.14041	-0.04633	0.65987	0.010767	0.012320	0.023893	-0.003728	0.000921	-0.003631	1.000	3
13	F 6	-0.05150	-0.08902	0.88331	0.012027	0.015329	0.039603	0.000723	-0.009841	-0.006361	1.000	3
14	S 04	0.30877	0.32824	0.97498	0.004542	0.006969	0.014738	-0.002509	0.003397	-0.003999	1.000	2
15	S 05	0.48472	0.22493	0.74653	0.002689	0.004129	0.011748	-0.001077	0.000989	-0.002700	1.000	2
16	S 06	0.49729	0.29188	0.22134	0.003983	0.004217	0.014503	-0.001910	0.001141	-0.000279	1.000	2
17	S 07	0.52012	0.42692	0.69955	0.004867	0.003002	0.013464	-0.000855	0.001468	-0.000473	1.000	2
18	S 08	0.46862	0.08127	0.28102	0.006607	0.004879	0.012597	-0.003723	0.003778	-0.002808	1.000	2
19	S011	0.62431	-0.02925	0.07788	0.008657	0.006036	0.028175	-0.004558	0.008051	-0.007613	1.000	2
20	S013	0.29345	0.18799	0.51415	0.006556	0.006395	0.015418	-0.003726	0.004414	-0.004610	1.000	2
21	S014	0.13402	0.27328	0.74424	0.010677	0.014025	0.015695	-0.008055	0.008171	-0.009990	1.000	2
22	S015	0.14442	0.41211	1.19234	0.007242	0.010250	0.022308	-0.005021	0.007179	-0.005562	1.000	2
23	S018	0.45695	0.21711	0.00568	0.005355	0.007279	0.013523	-0.003528	0.000958	-0.001041	1.000	2
24	S019	0.67684	0.35824	0.48160	0.004305	0.004933	0.013634	-0.001980	0.002673	0.001317	1.000	2
25	S022	0.63669	0.11469	0.53517	0.005833	0.007091	0.016278	-0.003437	0.000565	-0.001756	1.000	2
26	S030	0.32669	0.39523	0.45454	0.005360	0.004694	0.013532	-0.001202	0.002287	-0.000431	1.000	2
27	S031	0.17426	0.50269	0.67787	0.006507	0.008403	0.013865	-0.003057	0.001049	-0.004688	1.000	2
28	S032	0.19357	0.63601	1.15133	0.004988	0.006398	0.015228	-0.001296	0.003124	-0.003086	1.000	2
29	S033	0.34966	0.52731	0.94072	0.004244	0.004929	0.008794	-0.001866	0.002245	-0.001354	1.000	2
30	C012	0.23975	0.42483	1.08753	0.006955	0.005152	0.007780	-0.000775	-0.002697	0.001663	1.000	4
31	C024	0.21938	0.29643	0.61258	0.005124	0.007060	0.001874	-0.000767	0.000715	-0.005219	1.000	4
32	C033	0.59036	0.33115	0.59458	0.000683	0.003009	0.026567	-0.000174	-0.001446	-0.004605	1.000	4
33	C046	0.57761	0.23337	0.61638	0.001621	0.005046	0.004030	0.000082	0.001147	0.001169	1.000	4
34	C051	0.56324	0.19037	0.10609	0.001559	0.006216	0.003476	-0.001907	-0.002539	-0.000941	1.000	4
35	C053	0.56250	0.08771	0.14823	0.004047	0.002799	0.005593	-0.003232	0.002273	-0.000525	1.000	4
36	C060	0.23670	0.39113	0.58747	0.004430	0.003716	0.006117	-0.002754	0.000907	-0.000147	1.000	4
37	C061	0.43555	0.21536	0.31914	0.002403	0.005320	0.001676	-0.001279	-0.000780	-0.002371	1.000	4
38	C062	0.36337	0.26432	0.40991	0.002060	0.005061	0.027327	-0.002035	-0.000889	-0.000302	1.000	4
39	C063	0.38277	0.40183	0.88779	0.006053	0.007116	0.013633	-0.004727	0.002738	-0.002713	1.000	4
40	C064	0.45209	0.35388	0.78901	0.003871	0.007927	0.004774	-0.001388	-0.001296	-0.001166	1.000	4
41	C065	0.25834	0.52315	1.05662	0.007540	0.008713	0.016004	-0.005740	0.004496	-0.006975	1.000	4
42	C066	0.08577	0.57652	0.54377	0.008297	0.005757	0.031425	-0.000982	-0.000510	-0.003712	1.000	4
43	C067	0.11444	0.16984	0.67434	0.013759	0.018370	0.035719	-0.015090	0.011103	-0.010719	1.000	4
44	C068	0.70302	0.00680	-0.04963	0.005958	0.004728	0.013922	-0.001550	0.005128	-0.006658	1.000	4
45	C069	0.74330	0.09204	-0.00011	0.003631	0.004811	0.017431	-0.001896	0.000371	-0.003373	1.000	4
46	C070	0.10838	0.73477	1.01008	0.013617	0.008671	0.023681	0.001956	-0.023246	0.000555	1.000	4
47	C071	0.14744	0.28694	1.15527	0.012895	0.017411	0.038107	-0.014085	0.012791	-0.012049	1.000	4
48	C072	0.72896	0.14235	0.42733	0.005907	0.005755	0.009775	-0.002655	-0.000217	-0.001278	1.000	4
49	C073	0.75724	0.22855	0.46984	0.004380	0.005872	0.088119	-0.003594	0.016630	-0.012506	1.000	4
50	S 4	0.69004	0.67247	0.02133	0.004726	0.004218	0.016555	-0.002880	0.000925	-0.000130	1.000	2
51	S 5	0.51505	0.77476	0.25605	0.005276	0.004549	0.021710	-0.003209	0.002471	-0.000064	1.000	2
52	S 6	0.50128	0.70898	0.77294	0.004513	0.005018	0.015876	-0.002134	0.002567	-0.003581	1.000	2
53	S 7	0.48092	0.57113	0.29331	0.003089	0.004946	0.018782	-0.002433	0.003041	-0.003330	1.000	2
54	S 8	0.53201	0.91479	0.71966	0.004609	0.005788	0.016480	-0.002987	0.002822	-0.003409	1.000	2
55	S 11	0.37692	1.02701	0.92101	0.008880	0.006846	0.024918	-0.004318	0.009100	-0.007093	1.000	2
56	S 13	0.70630	0.81193	0.48328	0.006064	0.007173	0.017025	-0.004295	0.003388	-0.003079	1.000	2
57	S 14	0.86584	0.72282	0.26111	0.009594	0.013468	0.031857	-0.009038	0.009699	-0.009074	1.000	2
58	S 15	0.85450	0.58495	-0.19629	0.006893	0.010643	0.018494	-0.006089	0.004444	-0.005566	1.000	2
59	S 18	0.34236	0.77975	0.99503	0.004311	0.004514	0.013499	-0.002256	0.003205	-0.001053	1.000	2
60	S 19	0.32246	0.63980	0.51772	0.003895	0.005524	0.022427	-0.002009	0.002566	-0.003480	1.000	2
61	S 22	0.36195	0.88582	0.45990	0.004570	0.002441	0.017917	-0.000717	0.002861	-0.003488	1.000	2
62	S 30	0.67191	0.60725	0.54148	0.003394	0.005950	0.015594	-0.002716	0.001637	-0.004651	1.000	2
63	S 31	0.82662	0.49845	0.32011	0.005077	0.007589	0.017632	-0.002433	0.003743	-0.007216	1.000	2
64	S 32	0.80583	0.36247	-0.15593	0.006465	0.006611	0.012217	-0.003450	0.002318	-0.003364	1.000	2
65	S 33	0.64908	0.47380	0.05982	0.004588	0.003927	0.022680	-0.002059	0.002213	-0.001247	1.000	2
66	C 12	0.76494	0.56461	-0.07154	0.002555	0.006895	0.013247	-0.003329	0.004468	-0.004218	1.000	4
67	C 24	0.77671	0.70945	0.38417	0.005805	0.008514	0.029635	-0.006168	0.006181	-0.002913	1.000	4
68	C 33	0.40743	0.67478	0.40338	0.004848	0.004481	0.004740	-0.001607	0.003962	0.002043	1.000	4
69	C 46	0.42772	0.76728	0.37986	0.005051	0.003806	0.023400	-0.003222	0.000690	-0.003639	1.000	4
70	C 51	0.42121	0.81381	0.86251	0.001655	0.002986	-0.003052	-0.000253	-0.004142	0.000517	1.000	4
71	C 53	0.44550	0.90237	0.84541	0.006513	0.008570	0.018454	-0.000686	0.003949	-0.007975	1.000	4
72	C 60	0.76202	0.62126	0.40535	0.003723	0.011718	0.023267	-0.001642	0.004345	-0.011004	1.000	4
73	C 61	0.57429	0.77997	0.68054	0.004590	0.002221	0.035355	-0.001528	0.005222	-0.001300	1.000	4
74	C 62	0.64336	0.74235	0.58269	0.005285	0.004595	0.002529	-0.002157	0.003087	-0.001808	1.000	4
75	C 63	0.62408	0.60480	0.10784	0.001900	0.002844	0.011761	-0.000404	0.001477	-0.000220	1.000	4
76	C 64	0.54944	0.64230	0.20976	0.003553	0.001203	0.029431	-0.002043	0.004226	-0.002512	1.000	4
77	C 65	0.74459	0.47744	-0.06670	0.003028	0.003102	0.004427	0.000345	0.000433	0.002114	1.000	4
78	C 66	0.91211	0.43465	0.44705	0.007892	0.011991	0.015772	-0.001226	-0.003079	-0.005022	1.000	4
79	C 67	0.88586	0.84003	0.29957	0.016781	0.011930	0.023321	-0.010280	0.008797	-0.007093	1.000	4
80	C 68	0.28210	0.99960	1.04443	0.006350	0.014957	0.051904	-0.006018	0.007338	-0.002467	1.000	4
81	C 69	0.25536	0.92155	0.99726	0.006781	0.010066	0.052926	-0.003544	0.012640	-0.012752	1.000	4
82	C 70	0.88060	0.28473	-0.01143	0.005946	0.010382	0.021923	-0.001489	-0.005313	-0.004901	1.000	4
83	C 71	0.84988	0.71922	-0.17221	0.014833	0.010211	0.015701	-0.008099	0.006329	-0.005386	1.000	4
84	C 72	0.26815	0.84711	0.56608	0.004999	0.007639	0.061665	-0.002948	0.014090	-0.012449	1.000	4
85	C 73	0.23532	0.77679	0.51438	0.003446	0.008169	0.012751	0.000166	-0.003895	-0.003478	1.000	4

Table 3-9. The isotropic thermal factors, B_{eq}s, of alkyl carbon atoms in $(C_1TET\text{-}TTF)_4Sb_2F_{11}$. The values for the PF_6 salts are also listed for comparison.

$$B_{eq}=(4/3)\Sigma\Sigma B_{ij}a_i a_j \quad (i,j)$$

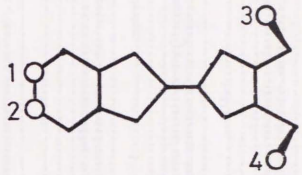

$B_{eq}/\AA^2$

		1	2	3	4
Sb_2F_{11}	A	2.93	3.48	5.51	4.98
	A'	8.93	9.77	3.69	6.09
	B	12.43	2.37	9.21	5.49
	B'	1.97	9.67	2.16	5.73
	average	6.56	6.32	5.14	5.57
PF_6-MeOH		11.85	10.05	9.02	7.56 10.34
PF_6-EtOH		8.62	7.79	7.64	7.43 6.75

Table 3-10. F_o-F_c for $(C_1TET\text{-}TTF)_4Sb_2F_{11}$.

Number of reflections=6774

Format:(h k l F_o F_c del)

Table 3-10. (continued)

Format:(h k l F_o F_c del)

Table 3-10. (continued)

Format:(h k l F_o F_c del)

Table 3-10. (continued)

Format:(h k l F_o F_c del)

Table 3-10. (continued)

Format:(h k l F_o F_c del)

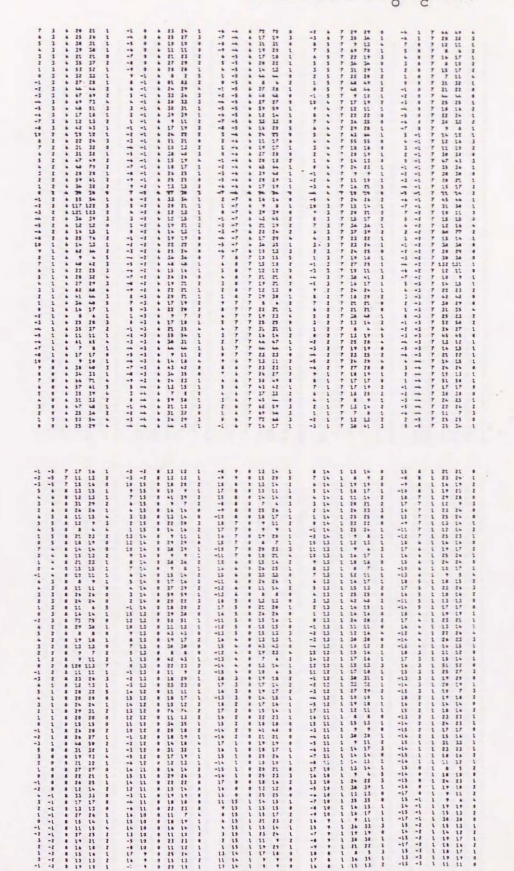

Table 3-10. (continued)

Format:(h k l F_o F_c del)

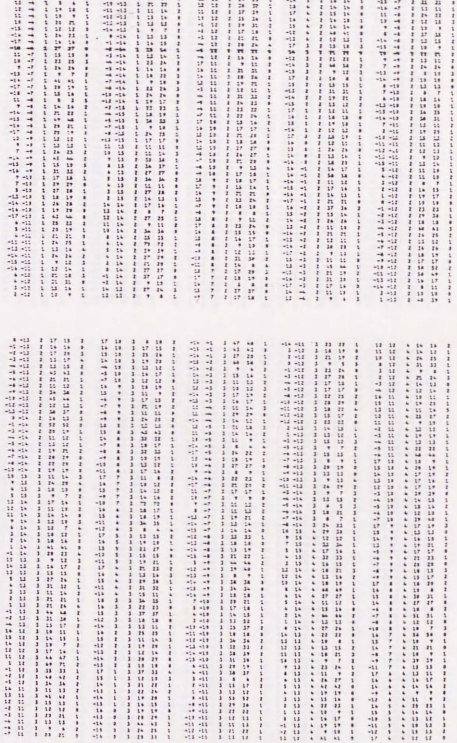

Table 3-10. (continued)

Format:(h k l F_o F_c del)

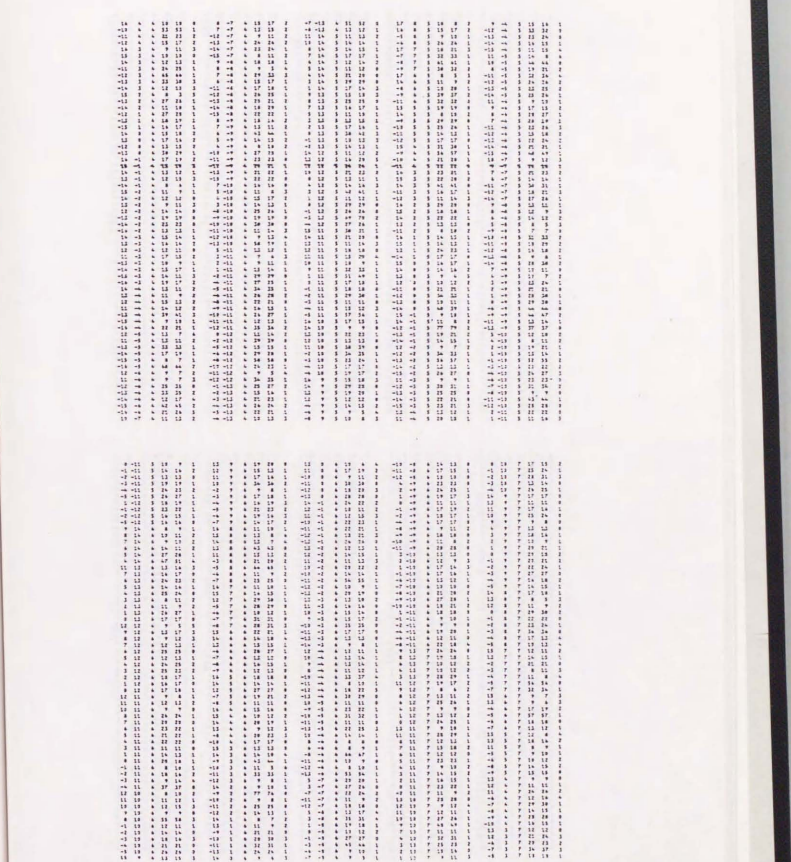

Table 3-10. (continued)

Format:(h k l F_o F_c del)

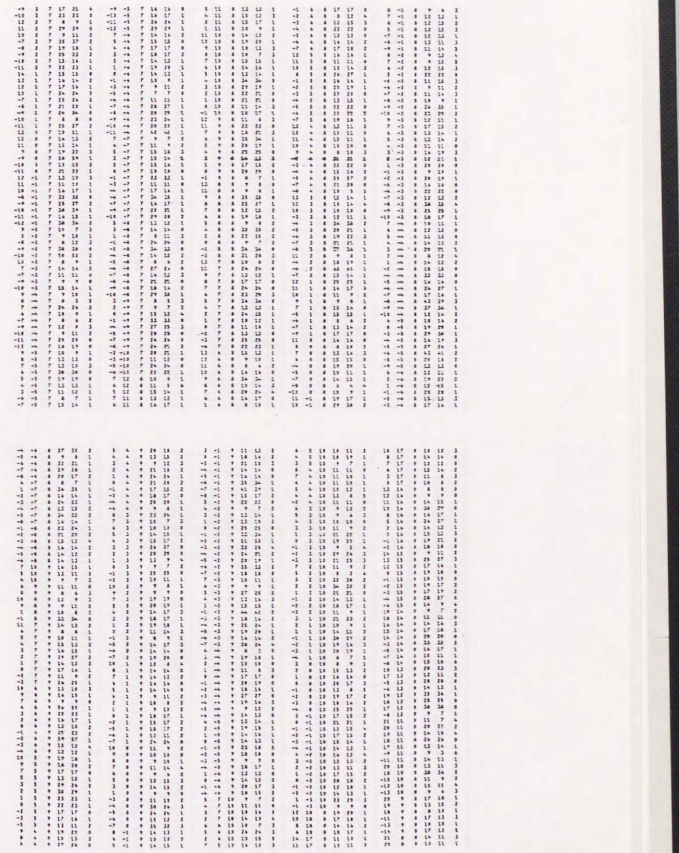

Table 3-10. (continued)

Format: (h k l F_o F_c del)

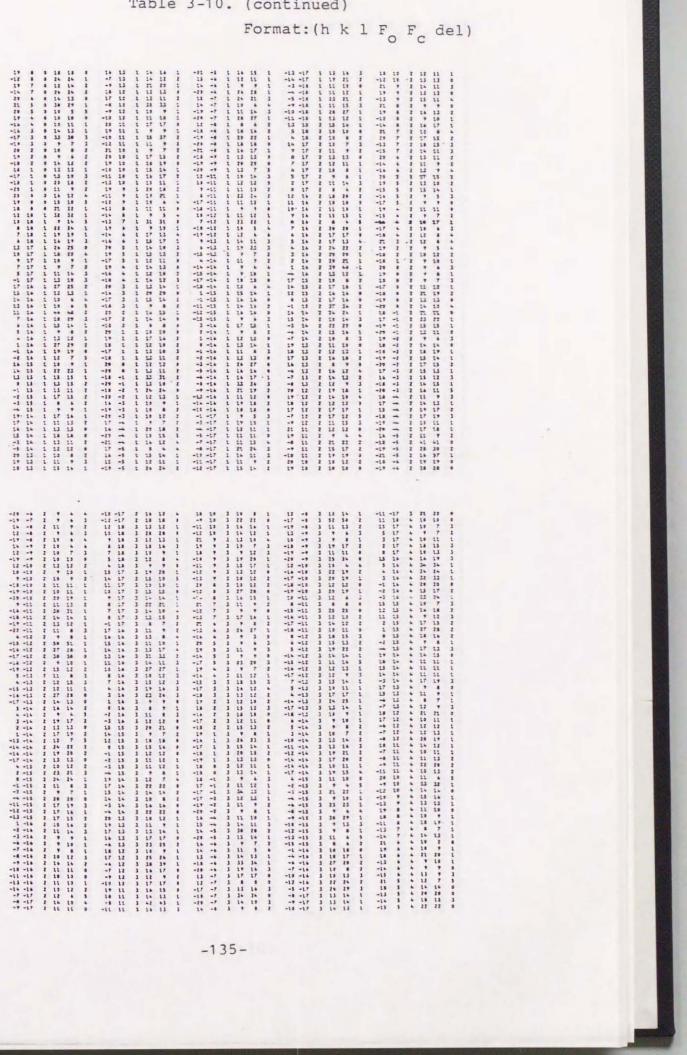

Table 3-10. (continued)

Format:(h k l F_o F_c del)

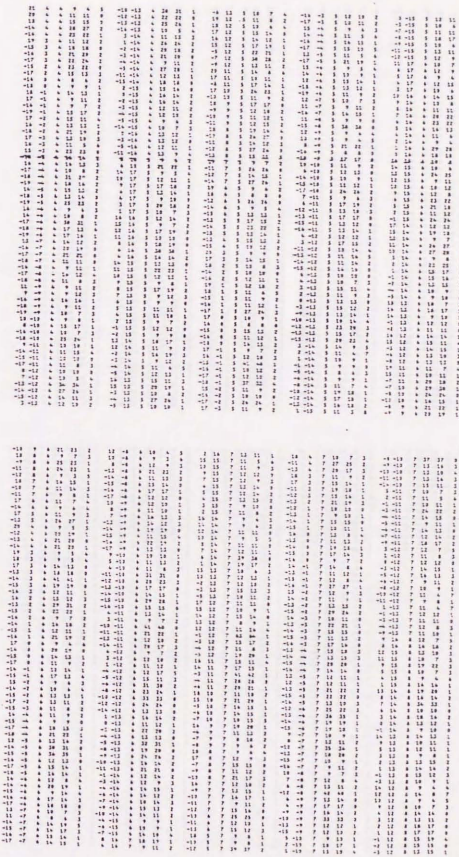

Table 3-10. (continued)

Format:(h k l F_o F_c del)

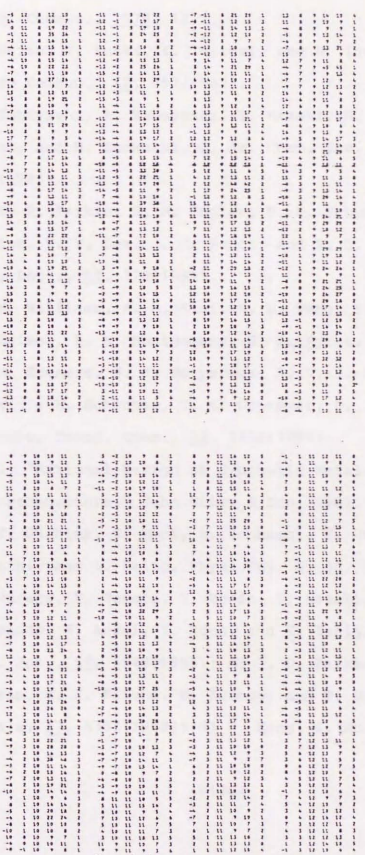

References

1) M. Mizuno, A. F. Garito, and M. P. Cava, J. Chem. Soc., Chem. Commun., 1978, 18.

2) G. Saito, T. Enoki, K. Toriumi, and H. Inokuchi, Solid State Commun., 42, 557(1982).

3) H. Kobayashi, A. Kobayashi, Y. Sasaki, G. Saito, T. Enoki, and H. Inokuchi, J. Am. Chem. Soc., 105, 297(1983).

4) S. S. P. Parkin, E. M. Engler, R. R. Schumaker, R. Lagier, V. Y. Lee, J. C. Scott, and R. L. Greene, Phys. Rev. Lett., 50, 270(1983).

5) J. M. Williams, A. M. Kini, H. H. Wang, K. D. Carlson, U. Geiser, L. K. Montgomery, G. J. Pyrka, D. M. Watkins, J. M. Kommers, S. J. Boryschuk, A. V. S. Crouch, W. K. Kwok, J. E. Schirber, D. L. Overmyer, D. Jung, and M. H. Whangbo, Inorg. Chem., 29, 3272(1990).

7) E.g., "Rational Design of Synthetic Metal Superconductors," John Wiley & Son, 1987.

8) a) K. Ohshima, T. Mori, H. Inokuchi, H. Urayama, H. Yamochi, and G. Saito, Phys. Rev. B, 38, 938(1988); b) K. Murata, N. Toyota, Y. Honda, T, Sasaki, M. Tokumoto, H. Bando, H. Anzai, Y. Muto, and T. Ishiguro, J. Phys. Soc. Jpn., 57, 1540(1988); c) I. D. Parker, D. D. Pigram, R. H. Friend, M. Kurmoo, and P. Day, Synthetic Metals, 27, A387(1988); d) W. Kang, G. Montamboux, J. R.

Cooper, D. Jerome, P. Batail, and C. Lenoir, Phys. Rev. Lett., 62, 2561(1989).

9) P. R. Moses and J. Q. Chambers, J. Am. Chem. Soc., 96, 945(1974).

10) P. Wu, T. Mori, T. Enoki, K. Imaeda, G. Saito, and H. Inokuchi, Bull. Chem. Soc. Jpn., 59, 127(1986).

11) P. Wu, G. Saito, K. Imaeda, Z. Shi, T. Mori, T. Enoki, and H. Inokuchi, Chem. Lett., 1986, 441.

12) K. Imaeda, T. Enoki, Z. Shi, P. Wu, N. Okada, H. Yamochi, G. Saito, and H. Inokuchi, Bull. Chem. Soc. Jpn., 60, 3163(1987).

13) a) Z. Shi, T. Enoki, K. Imaeda, K. Seki, P. Wu, H. Inokuchi, and G. Saito, J. Phys. Chem., 92, 5044(1988); b) P. Wang, T. Enoki, K. Imaeda, N. Iwasawa, H. Yamochi, H. Urayama, G. Saito, and H. Inokuchi, J. Phys. Chem., 93, 5947(1989).

14) a) K. Seki, T. B. Tang, T. Mori, P. Wu, G. Saito, and H. Inokuchi, J. Chem. Soc., Faraday Trans. 2, 82, 1067(1986); b) H. Yamamoto, K. Seki, H. Inokuchi, and G. Saito, J. Chem. Soc., Faraday Trans. 2, 83, 2151(1987).

15) A. Otsuka, G. Saito, T. Nakamura, M. Matsumoto, Y. Kawabata, K. Honda, M. Goto, and M. Kurahashi, Synthetic Metals, 27, B575(1988).

16) R. Schumaker, V. Lee, and E. Engler, J. Org. Chem., 49, 564(1984).

17) G. Steimecke, H. Sieler, R. Kirmse, and E. Hoyer, Phosphorus and Sulfur, 7, 49(1979).

18) D. G. Anderson, J. C. Smith, and R. J. Rallings, J. Chem. Soc., 1953, 443.

19) G. C. Papavassiliou, G. A. Mousdis, S. Y. Yiannopoulos, V. C. Kakoussis, and J. S. Zambounis, Synthetic Metals, 27, B373(1988).

20) A private communication from G. C. Papavassiliou at the first ISSP International Symposium on the Physics and Chemistry of Organic Superconductors, Tokyo, Japan, August 28-30, 1989.

21) a) C. Katayama, M. Honda, H. Kumagai, J. Tanaka, G. Saito, and H. Inokuchi, Bull. Chem. Soc. Jpa., 58, 2272(1985); b) H. Endres, Z. Naturforsch., Teil B, 41, 1351(1986).

22) H. Yamochi, N. Iwasawa, H. Urayama, and G. Saito, Chem. Lett., 1987, 2265.

23) N. Iwasawa, G. Saito, K. Imaeda, T. Mori, and H. Inokuchi, Chem. Lett., 1987, 2399.

24) N. Iwasawa, Doctor's Thesis, The University of Tokyo(Japan)1987.

25) H. Inokuchi, K. Imaeda, T. Enoki, T. Mori, Y. Maruyama, G. Saito, N. Okada, H. Yamochi, K. Seki, Y. Higuchi, and N. Yasuoka, Nature, 329, 39(1987).

26) H. Kobayashi, A. Kobayashi, Y. Sasaki, G. Saito, and H.

Inokuchi, Bull. Chem. Soc. Jpn., 59, 301(1986).

27) G. Saito, H. Kumagai, C. Katayama, C. Tanaka, J. Tanaka, P. Wu, T. Mori, K. Imaeda, T. Enoki, H. Inokuchi, Y. Higuchi, and N. Yasuoka, Isr. J. Chem., 27, 319(1986).

28) N. Sato, G. Saito, and H. Inokuchi, Chem. Phys., 76, 79(1983).

29) H. Tatemitsu, E. Nishikawa, Y. Sakata, and S. Misumi, J. Chem. Soc., Chem. Commun., 1985, 106.

30) a) G. Saito, Physica, B, 143, 296(1986); b) G. Saito, Pure Appl. Chem., 59, 999(1987).

31) J. Richard, M. Vandevyver, A. Barraud, J. P. Morand, R. Lapouyade, P. Delhaes, J. F. Jacquinot, and M. Roulliay, J. Chem. Soc., Chem. Commun., 1988, 754.

32) T. Mori, A. Kobayashi, Y. Sasaki, R. Kato, and H. Kobayashi, Chem. Lett., 1984, 1335.

33) a) M. Narita and C. U. Pittman, Synthesis, 1976, 489; b) A. Krief, Tetrahedron, 42, 1209(1986); c) G. Schukat, A. M. Richter, and E. Fanghanel, Sulfur Reports, 7, 155(1987).

34) P. Wu and X. Zheng, Proceedings of 2nd China-Japan Joint Symposium on Conduction and Photo-Conduction in Organic Solids and Related Phenomena, Institute for Molecular Science, Okazaki, November 18-20, 1986. p.69.

35) G. Saito, H. Hayashi, T. Enoki, and H. Inokuchi, Mol. Cryst. Liq. Cryst., 120, 341(1985).

36) a) T. Mori and H. Inokuchi, Solid State Commun., 59, 355(1986); b) T. Mori and H. Inokuchi, Bull. Chem. Soc. Jpn., 60, 402(1987).

37) K. Imaeda, T. Mori, C. Nakano, H. Inokuchi, N, Iwasawa, and G. Saito, submitted to Bull. Chem. Soc. Jpn.

38) A. Otsuka, Master's Thesis, The University of Tokyo(Japan)1988.

39) D. Zhu, X. Wu, Y. Liu, X. Wang, Y. Hua, X. Pang, and D. Jiang, the abstract book of the 4th International Conference on Langmuir-Blodgett Films, Tsukuba, Japan, April 24-29, 1989. EP-4(p.366).

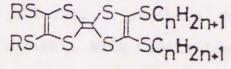

RR=-CH_2CH_2-, n=16
RR=-CH_2CH_2-, n=18
R=CH_3, n=16

40) C. Lalanne, P. Delhaes, E. Dupart, Ch. Garrigou-Lagrange, J. Amiell, J. P. Morand, and B. Desbat, Thin Solid Films, 179, 171(1989).

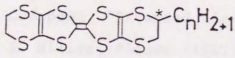

BEDT-TTFC$_n$
(n=16, 18, 20)

41) R. P. Shibaeva, R. M. Lobkovskaya, L. P. Rozenberg, L. I. Buravov, A. A. Ignatiev, N. D. Kushch, E. E. Laukhina, M. K. Makova, E. B. Yagubskii, and A. V. Zvarykina, Synthetic Metals, 27, A189(1988).

42) H. Kobayashi, T. Mori, R, Kato, A. Kobayashi, Y. Sasaki,

G. Saito, and H. Inokuchi, Chem. Lett., 1983, 581.

43) G. Keryer, J. Amiell, S. Flandrois, P. Delhaes, E. Toreilles, J. M. Fabre, and L. Giral, Solid State Commun., 26, 541(1978).

44) T. Nakamura, G. Saito, T. Inukai, T. Sugano, M. Kinoshita, and M. Konno, Solid State Commun., 75, 583(1990).

45) M. Z. Aldoshina, L. O. Atovmyan, L. M. Goldenberg, O. N. Krasochka, R. N. Lubovskaya, R. B. Lubovskii, V. A. Merzhanov, and M. L. Khidekel, J. Chem. Soc., Chem. Commun., 1985, 1658.

46) K. Kikuchi, Y. Ishikawa, K. Saito, I. Ikemoto, and K. Kobayashi, Acta Crystallogr., C, 44, 466(1988).

47) H. Kobayashi, R. Kato, T. Mori, A. Kobayashi, Y. Sasaki, G. Saito, T. Enoki, and H. Inokuchi, Mol. Cryst. Liq. Cryst., 107, 33(1984).

48) H. Endres, Z. Naturforsch., Teil B, 41, 1437(1986).

49) P. Copppens, "Extended Linear Chain Compounds I," ed by J. S. Miller, Plenum (1982), p.333.

50) a) K. O. Christe, C. J. Schack, and R. D. Wilson, Inorg. Chem., 15, 1275(1976); b) B. Bonnet and G. Mascherpa, ibid., 19, 785(1980); c) N. C. Craig, R. K. -Y. Lai, K. W. Penfield, and I. W. Levin, J. Phys. Chem., 84, 899(1980).

51) J. Bacon, P. A. W. Dean, and R. J. Gillespie, Can. J.

Chem., 47, 1655(1969).

52) C. Lenoir, K. Boubekeur, P. Batail, E. Canadell, P. Auban, O. Traetteberg, and D. Jerome, Synthtic Metals, in press.

53) T. Mori, Fukuoka, October 13-16, 1990. 3bP26(p.452).

54) a) V. M. McRae, R. D. Peacock, and D. R. Russell, J. Chem. Soc., Chem. Commun., 1969, 62; b) W. Clegg, O. Glemser, K. Harms, G. Hartmann, R. Mews, M. Noltemeyer, and G. Sheldrick, Acta Crystallogr., B, 37, 548(1981).

55) F. A. Cotton and G. Wilkinson, "Advanced Inorganic Chemistry," 5th edition, John Wiley & Sons, (1988), p.398.

56) T. Sugano, G. Saito, and M. Kinoshita, Phys. Rev. B, 35, 6554(1987).

57) E. L. Venturini, J. E. Schirber, H. H. Wang, and J. M. Williams, Synthetic Metals, 27, A243(1988).

58) Y. Higuchi, K. Inaka, N. Yasuoka, and C. Nakano, private communication.

59) J. C. Scott, A. F. Garito, and A. J. Heeger, Phys. Rev. B, 10, 3131(1974).

60) F. Wudl, D. E. Schafer, W. M. Walsh, L. W. Rupp, F. J. DiSalvo, J. V. Waszczak, M. L. Kaplan, and G. A. Thomas, J. Chem. Phys., 66, 377(1977).

61) V. F. Kaminskii, M. L. Khidekel, R. B. Lyubovskii, I. F. Shchegolev, R. P. Shibaeva, E. B. Yagubskii, A. V.

Zvarykina, and G. L. Zvereva, Phys. Status Solidi A, 44, 77(1977).

62) P. Delhaes, C. Coulon, J. Amiell, S. Flandrois, E. Toreilles, J. M. Fabre, and L. Giral, Mol. Cryst. Liq. Cryst., 50, 43(1979).

63) J. C. Scott, H. J. Pedersen, and K. Bechgaard, Phys. Rev. Lett., 45, 2125(1980).

64) J. C. Scott, "Semiconductors and Semimetals, Vol. 27," ed by E. Conwell, Academic Press (1988), p.400.

65) D. B. Chestnut and W. D. Phillips, J. Chem. Phys., 35, 1002(1961).

66) J. C. Bonner and M. E. Fisher, Phys. Rev. A, 135, 640(1964).

67) a) W. Duffy, Jr. and K. P. Barr, Phys. Rev., 165, 647(1968); b) J. N. Fields, H. W. J. Blöte, and J. C. Bonner, J. Appl. Phys., 50, 1807(1979); c) J. C. Bonner, H. J. W. Blöte, J. W. Bray, and I. S. Jacobs, ibid., 50, 1810(1979).

68) F. D. Rossini, K. S. Pitzer, R. L. Arnett, R. M. Braun, G. C. Pimentel, "Selected Values of Physical and Thermodynamic Properties of Hydro Carbons and Related Compounds," Pittsburgh (1953).

69) For n=1 and 3~10: F. D. Rossini, K. S. Pitzer, R. L. Arnett, R. M. Braun, G. C. Pimentel, "Selected Values of Physical and Thermodynamic Properties of Hydro Carbons

and Related Compounds," Pittsburgh (1953); n=2: R. K. Witt and J. D. Kemp, J. Am. Chem. Soc., 59, 273(1937); n=11~18: A. J. Streiff, A. R. Hulme, P. A. Cowie, N. C. Krouskop, and F. D. Rossini, Anal. Chem., 27, 411(1955); n=19~25: A. A. Schaerer, C. J. Busso, A. E. Smith, and L. B. Skinner, J. Am. Chem. Soc., 77, 2017(1955).

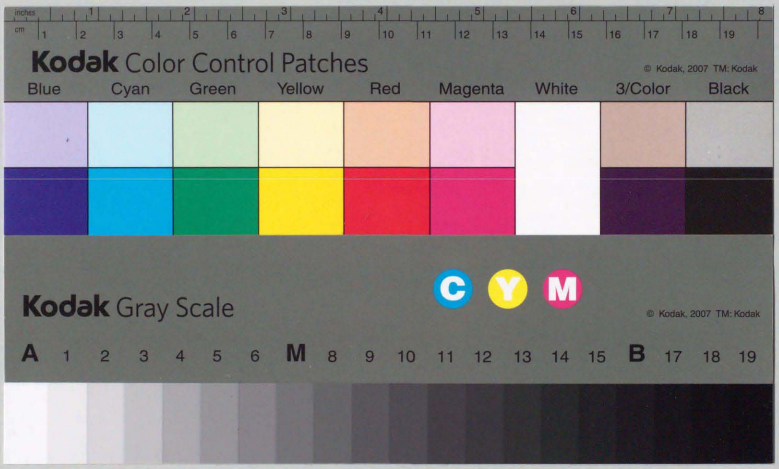
inches
cm
Kodak Color Control Patches
© Kodak, 2007 TM: Kodak
Blue
Cyan
Green
Yellow
Red
Magenta
White
3/Color
Black
C
Y
M
Kodak Gray Scale
© Kodak, 2007 TM: Kodak
A 1 2 3 4 5 6 M 8 9 10 11 12 13 14 15 B 17 18 19